ABSTRACT

AFROZ, TALIMAN. Molecular-level Interactions in Li-ion Battery Electrolytes: Linear Solvent-$LiClO_4$ Mixtures. (Under the direction of Wesley A. Henderson).

The performance of Li-ion batteries depends significantly on the composition and properties of the electrolytes. Very limited information is available, however, about the molecular-level interactions within the electrolytes which, in turn, influence bulk electrolyte properties such as viscosity and ionic conductivity. Vibrational spectroscopic and thermal analysis of organic solvent-lithium salt systems has therefore been carried out to better understand how the choice of solvent and salt, as well as salt concentration and temperature, influence the molecular-level interactions in electrolytes. In particular, the study of linear carbonate- and carboxylic ester-$LiClO_4$ mixtures, through the generation of phase diagrams and a Raman spectroscopic analysis, provides significant insight regarding the types of solvates present and the degree of ionic association occurring within these mixtures. Further, X-ray diffractional analysis of the single crystal solvate structures formed in these mixtures provides important information about the coordination of the Li^+ cations by the solvent molecules and anions. The linear solvents studied include diethyl carbonate (DEC), dimethyl carbonate (DMC), methyl acetate (MA) and ethyl acetate (EA). To aid in the analysis, a detailed Raman spectroscopic analysis has also been conducted to characterize $LiClO_4$ solvates with known structures to unambiguously assign the Raman bands to specific forms of ClO_4^- coordination to Li^+ cations to aid in properly identifying the solvates present in the liquid mixtures.

Molecular-level Interactions in Li-ion Battery Electrolytes: Linear-Solvent-$LiClO_4$ Mixtures

by
Taliman Afroz

A thesis submitted to the Graduate Faculty of
North Carolina State University
in partial fulfillment of the
requirements for the degree of
Master of Science

Chemical Engineering

Raleigh, North Carolina

2011

APPROVED BY:

_____	_____
Wesley A. Henderson Committee Chair	Saad Khan
_____	
Edmond F. Bowden	

BIOGRAPHY

Taliman Afroz was born on February 6, 1984 in Dhaka, Bangladesh. After graduating from Maple Leaf International School in 2001, she attended Bangladesh University of Engineering & Technology (BUET) for her undergraduate studies. In 2007, she graduated with her Bachelor of Science in Chemical Engineering from BUET. She joined the Department of Chemical & Biomolecular Engineering at North Carolina State University as a graduate student in the Fall semester of 2009.

ACKNOWLEDGMENTS

First I would like to thank my advisor Dr. Wesley A. Henderson for his guidance and support. There were numerous times when his encouraging words helped me to boost up my confidence.

I would also like to thank all the group members for providing a friendly working atmosphere. I owe my thanks especially to Daniel Seo who helped me to get acquainted with the instruments at the beginning. I would also like to thank Michael O'Connell for helping me with my research.

I gratefully acknowledge the help I got from all the staff of the Chemical & Biomolecular Engineering Department. I would specially like to thank Sandra Bailey for being so nice and helpful.

Finally, I would like to thank my parents, my brothers and my husband, Rashed, for their unconditional love and support.

TABLE OF CONTENTS

LIST OF TABLES

LIST OF FIGURES

Chapter 1. Introduction

1.1 Motivation

Tailoring the composition and properties of electrolytes is crucial for the performance of Li-ion batteries.[1] Current state-of-the-art electrolytes, which consist of mixtures of a lithium salt and two aprotic solvents, have many drawbacks,[1,2] and are not optimized for new electrode materials or for demanding applications such as large battery packs for plug-in hybrid vehicles (PHEVs). The current optimization method for electrolytes is based on a trial-and-error approach.[3] Very limited information is available about the interactions between the Li^+ cations, anions and the solvent molecules within electrolytes which, in turn, influence bulk electrolyte properties such as viscosity and ionic conductivity.[4,5] Polarity parameters such as dielectric constant, donor number and acceptor number are generally used to explain such interactions occurring within the electrolytes.[6] There are, however, instances which illustrate the limitations of such parameters in explaining the complex interactions occurring within such systems.[7,8] Thus, in the present study molecular-level interactions of aprotic solvent-lithium salt (LiX) systems were analyzed by experimentally determining the kind of solvate species present in the mixtures. This research provides significant information to aid in determining how solvent and anion structures govern the solvation of Li^+ cations in solvent-LiX mixtures. In addition to providing a fundamental understanding of the electrolyte systems, this study can be used as a guide to rapidly gauge the properties of new materials for electrolytes for a wide variety of Li-ion batteries and other applications.

1.2 Background

1.2.1 Lithium-Ion Batteries: Working Principle and Applications

Over the last few years, there has been a rapid increase in the demand for Li-ion batteries. Long cycle life, high energy density and light weight make them the popular choice for use in cell phones, laptop computers and other consumer products. Also, large Li-ion battery packs are increasingly being used in space vehicles, satellites and electric or hybrid electric vehicles.

A conventional Li-ion battery consists of a graphite anode, a lithium metal oxide cathode (such as $LiCoO_2$, $LiMn_2O_4$ or $LiNiO_2$), an electrolyte containing Li^+ cations, and a microporous separator.[9] Figure 1-1 shows a schematic diagram of a Li-ion battery. This battery functions using reversible chemistry, as represented by the 'intercalation' or 'insertion' type electrodes. This concept was first introduced by Wittingham[10,11] and later improved upon significantly by Goodenough *et al.* and others.[12,13] When the battery is being charged, the lithium metal oxide (positive electrode) is oxidized and the graphite anode (negative electrode) is reduced. In parallel, the Li^+ cations are subsequently deintercalated from the cathode material and intercalated into the graphite lattice. The mechanism

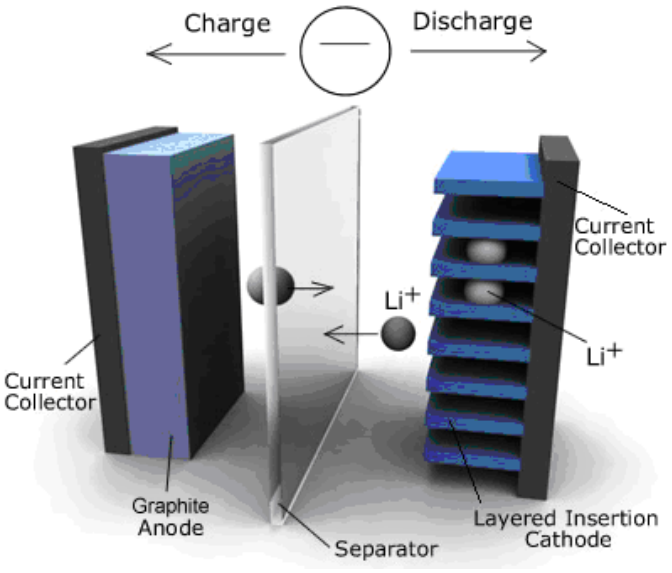

Figure 1-1. Schematic diagram of a Li-ion battery.

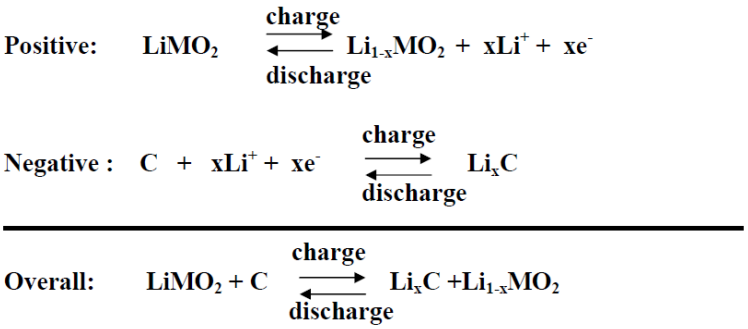

Figure 1-2. Electrode and cell reactions in a Li-ion battery.[2]

is reversed when the battery is discharged. Figure 1-2 shows the reactions taking place in the anode and the cathode during charging and discharging.[2]

Li-ion batteries have a number of advantages, such as high specific energy (~150 Wh kg^{-1}), high energy density (~400 Wh kg^{-1}), low discharge rate (2-8% per month) and long cycle life (more than 1000 cycles). In addition, Li-ion batteries can operate over a wide temperature range (-10°C to +50°C), making them suitable for most consumer purposes. The disadvantages, however, are mainly related to the safety hazards associated with them, especially at higher temperatures. At elevated temperature, usually above 130-150°C, exothermic chemical reactions can occur between the electrodes and electrolyte, which in turn can trigger more chemical reactions, ultimately leading to thermal runway.[14,15] In addition to the reactions between the electrodes and electrolyte, thermal runway can also be due to the thermal decomposition of the electrolyte, thermal decomposition of the electrodes or melting of the separator causing an internal short circuit.[18] Further, electrical (overcharge, high pulse power) or mechanical (crushing, internal or external short circuit) abuse can also lead to thermal runway.[15,16]

1.2.2 Electrolyte Materials

There are four major types of electrolytes used in Li-ion batteries: liquid electrolytes, gel electrolytes, polymer electrolytes and ceramic electrolytes.[2] Liquid electrolytes are solutions of a lithium salt in a mixture of organic solvents. Polymer electrolytes are formed by dissolving a salt in a high molecular weight polymer and gel electrolytes consist of a salt and a solvent dissolved or mixed with a high molecular weight polymer. Ceramic electrolytes, in contrast, are inorganic, solid-state materials that are ionically conductive. This work will focus on liquid electrolytes only.

1.2.3 State-of-the Art Liquid Electrolytes

Current Li-ion electrolyte systems generally use a binary solvent mixture of ethylene carbonate (EC) and a linear carbonate (e.g., diethyl carbonate (DEC)) with $LiPF_6$ (lithium hexafluorophosphate) as the lithium salt.[2] Such electrolytes have a high ionic conductivity (> 10^{-3} S cm^{-1}) and high lithium ion transference number (~0.35). $LiPF_6$, in combination with EC, reacts with the graphite anode to form a protective layer known as a SEI (solid electrolyte interface) on the anode. This layer prevents further decomposition of the electrolyte, but allows the transportation of Li^+ cations.[1] Also, at high potentials, $LiPF_6$ passivates aluminium (Al) (universally used commercially as the current collector for the cathode) preventing further corrosion of the Al.[17-19] This electrolyte composition, however, also has some disadvantages. $LiPF_6$ is hygroscopic and produces hydrofluoric acid upon reaction with water. Thus, it needs to be handled in a dry environment. Also at a temperature

lower than -10°C, the viscosity rapidly increases due to the EC with the concurrent reduction of the conductivity of the Li^+ cations. At temperatures higher than 50°C, various decomposition reactions occur within the battery between $LiPF_6$ and the solvent. Even though the specified temperature range is sufficient for use in consumer electronics, it limits the use of Li-ion technology for applications such as military and space uses, as well as hybrid and electric vehicles.[1]

1.2.4 Ion Solvation & Factors Affecting Ion Solvation

The term 'solvation' refers to "the surrounding of each dissolved molecule or ion by a shell of more or less tightly bound solvent molecules."[6] When a salt is dissolved in a solvent, energy is used to overcome the lattice energy of the crystals. This is compensated by the gain in Gibbs energy of solvation, ΔG^o_{solv}. Figure 1-3 shows the relationship between the standard molar Gibbs energies of solvation and solution and the crystal lattice energy of a salt represented by $(A^+B^-)_{solid}$. LiX salts such as $LiNO_3$, $LiCF_3SO_3$ and $LiClO_4$, however, are not

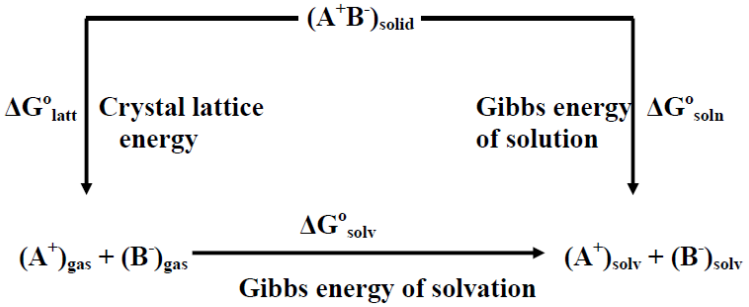

Figure 1-3. The relationship between standard molar Gibbs energies of solvation and solution and the crystal lattice.[6]

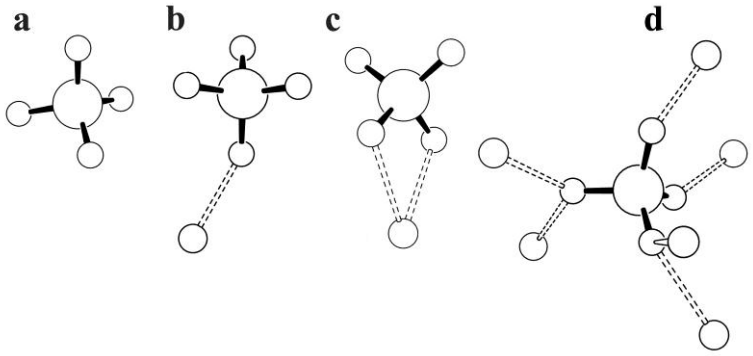

Figure 1-4. $Li^+ \ldots ClO_4^-$ coordination in $LiClO_4$ solvates: (a) SSIP, (b) CIP-I, (c) CIP-II and (d) AGG-III.

always fully solvated to form 'free' ions in solution. Aggregate (AGG) or contact-ion pair (CIP) solvates are formed if only some of the coordinating anions are replaced by the solvent molecules. CIPs[20-23] consist of the anion coordinated to one Li^+ cation, while AGGs are formed when the anions are coordinated to two (AGG-I)[24-27] or more than two (AGG-II, AGG-III)[28,29] Li^+ cations. If the anion remains uncoordinated and the Li^+ cations are fully solvated by the solvent molecules, then solvent-separated ion pairs (SSIPs)[30-38] are formed (Figure 1-4). Figure 1-5 shows the Li^+ cation solvates formed in tetrahydrofuran (THF) mixtures. There are a number of factors that influence the formation of different kinds of solvates in solvent-lithium salt mixtures. One of the main factors is the structure of the solvent. The donor number, DN,[39] is a measure of the ability of a solvent to donate electrons and the strength of the $D \ldots Li^+$ coordination bond (where D denotes the donor atom of the solvent molecule) is influenced by the type of donor atom. Oxygen and sulfur atoms, for example, have two electron lone pairs and thus can coordinate two separate Li^+ cations,

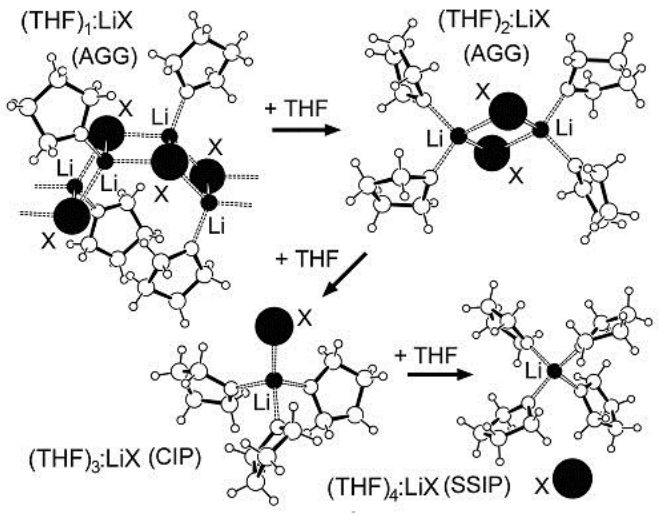

Figure 1-5. Li^+ cation solvates in THF-LiX mixtures (X is the anion).

whereas nitrogen with one lone pair can coordinate only a single Li^+ cation. Flexibility of the solvent molecules and temperature are also critical factors for ion solvation. Lithium cuprates, for example, form an equilibrium between SSIPs and CIPs in THF and diethyl ether (Et_2O) (the equilibrium being more pronounced at lower temperature), but THF mixtures predominantly contain SSIPs, whereas Et_2O mixtues mainly contain CIPs.[40-42] This, despite the fact that Figure 1-6 shows that the Li^+ cation solvates in Et_2O mixtures resemble those found in THF mixtures (Figure 1-5). Even though THF and Et_2O have similar structures (Figure 1-7) and coordinate the Li^+ cations through the oxygen lone pairs, the cyclic structure of THF forms stronger coordination with the Li^+ cations, thereby shielding the anions more effectively from cation coordination. Et_2O, on the other hand, has an open structure and because of the flexible ethyl groups can adopt several different conformations.[43] The Et_2O

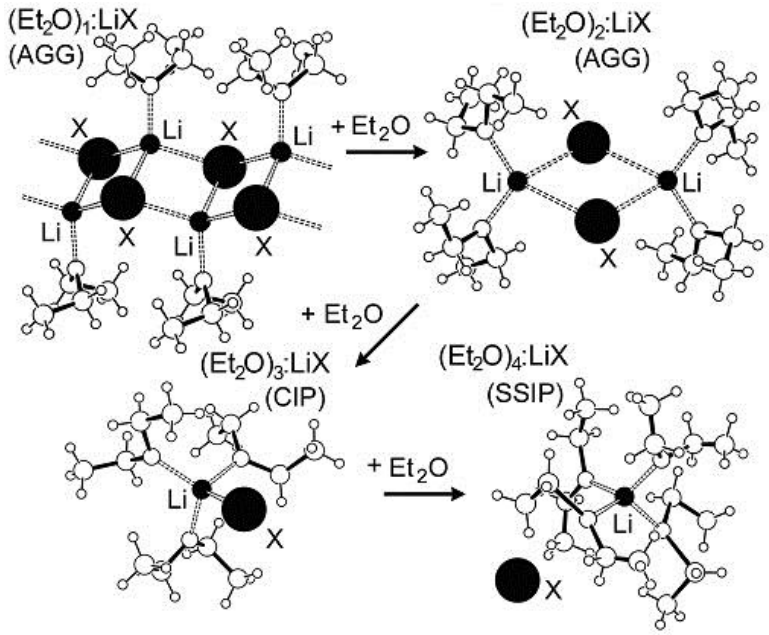

Figure 1-6. Li^+ cation solvates in Et_2O-LiX mixtures.

molecules are thus loosely bound around the Li^+ cations making it easier for the anions to approach the Li^+ cations. At lower temperatures, the flexible ethyl groups have reduced thermal energy and so a more efficient packing of the molecules and ions occurs.

Further, there are some solvent molecules that have more than one point of attachment; that is, a single solvent molecule can coordinate a Li^+ cation with more than one donor atom.[44] Such multidentate ligands (e.g., monoglyme (G1)) are better at coordinating Li^+ cations as compared to monodentate ligands (e.g., THF). For the same reason, diglyme (G2) coordinates Li^+ cations more strongly than G1.[45,46] Figure 1-7 shows the structures of G2, G1 and THF for comparison. The coordinate bond formed between the Li^+ cation and the donor atom is not static, but rather breaks and reforms with the same or different donor atoms from

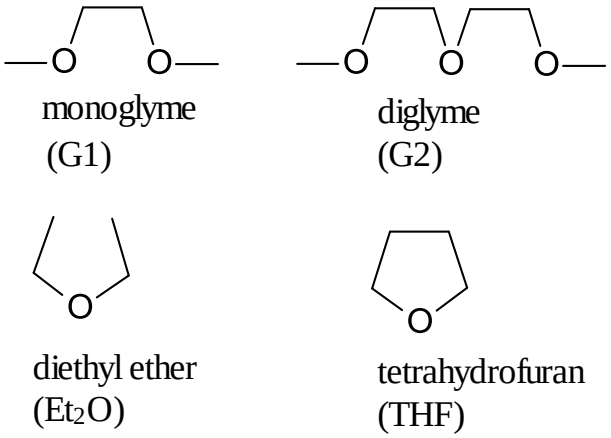

Figure 1-7. Structures of G1, G2, THF and Et_2O.

neighboring solvent molecules. The strength of bonding increases for multidentate ligands. This is because in the case of multidentate ligands, even though one coordinate bond is broken, the Li^+ cation is still coordinated with the other donor atom(s). This helps to keep the solvent molecule near the cation and decreases the chance that Li^+ cations will form new bonds with another solvent molecule or anion. Thus, the probability that the broken bond is reformed increases which, in turn, increases the stability of the solvate.

In addition to the solvent structures, solvate formation is also influenced by the anion properties because solvate formation depends on the balance between cation-solvent and cation-anion interactions. The coordinating ability of the anion is determined by the electronegativity of the donor atoms, steric effects and flexibility of the anions. If the anions are flexible, then they can adopt different conformations, allowing more variability in the manner in which the Li^+ cation can be coordinated by he anion. The

bis(trifluoromethanesulfonyl)imide ($N(SO_2CF_3)_2^-$ or $TFSI^-$) anion has two low energy conformers and there are numerous ways it can coordinate Li^+ cations.[50,51] Anions with high charge delocalization such as PF_6^-, AsF_6^- and $TFSI^-$ are poorly coordinating[52] because charge delocalization reduces the tendency for any one atom of the anion to preferentially interact with a single Li^+ cation. The size of the anion can also influence the cation-anion interaction if the size is large enough to prevent solvent molecules or other anions from approaching a Li^+ cation. The bis(perfluoroethanesulfonyl)imide ($N(SO_2C_2F_5)_2^-$ or $BETI^-$) anion, for example, forms a CIP-I solvate with triglyme (G3), but because of its large size the CIP-I structure has one Li^+ cation coordinated to one G3 molecule (four ether oxygens from one G3) thus differing from the two G3 molecules (two ether oxygens from each G3) in other $(G3)_1$:LiX solvates (Figure 1-8).[50,51]

The degree of ion solvation is also dependent on the concentration (solvent to salt ratio) of the mixtures. If the salt concentration increases, the number of solvent molecules decreases which means that there is decreased competition between the anions and the solvent molecules for coordination to the Li^+ cations. More anions surround the cations and so the ionic association increases with increasing salt concentration.[49] This study, therefore, aims to understand the intermolecular interactions occurring in aprotic solvent-LiX systems taking all the above described factors into consideration. The overall goal is to develop a comprehensive understanding of electrolyte solution structure.

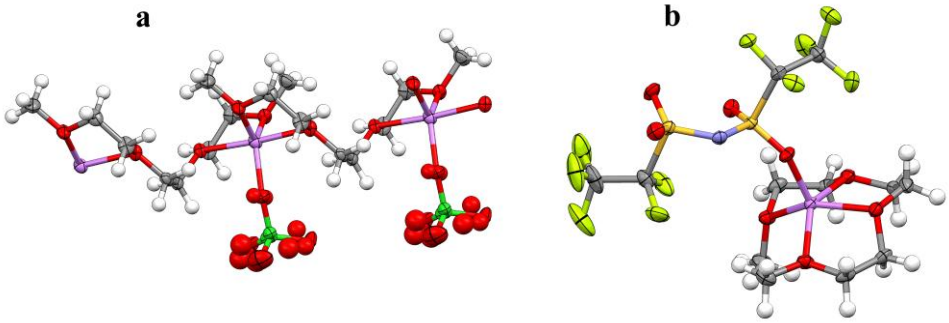

Figure 1-8. Li^+ cation coordination in crystalline solvate structures: (a) $(G3)_1$:$LiClO_4$ and (b) $(G3)_1$:LiBETI (Li – purple, O – red, Cl – dark green, N – blue, F – light green).[53,54]

1.3 Approach

Understanding the structure of liquids is among the most difficult tasks of physical chemistry. A combination of thermal, spectroscopic and x-ray structural analysis methods have therefore been used in conjunction to understand the complex nature of liquid electrolytes.[49,50,51-54]

For the thermal characterization of solvent-LiX systems, phase diagrams were generated from differential scanning calorimetry (DSC) data. Phase diagrams provide information about the kind of crystalline solvates present in the mixtures and the variation in phases with temperature and composition. Also, from the phase diagrams, it is possible to know the temperature range over which the mixture remains liquid and this, in turn, gives information about the solubility limit of a salt in a particular solvent. Figure 1-9 gives an example of DSC heating traces and the corresponding phase diagram for acetonitrile $(AN)_n$-$LiClO_4$ mixtures.[55] The peak temperatures in the DSC data are the melting points (T_m) of the mixtures. These temperatures are plotted against the corresponding lithium salt compositions to produce the

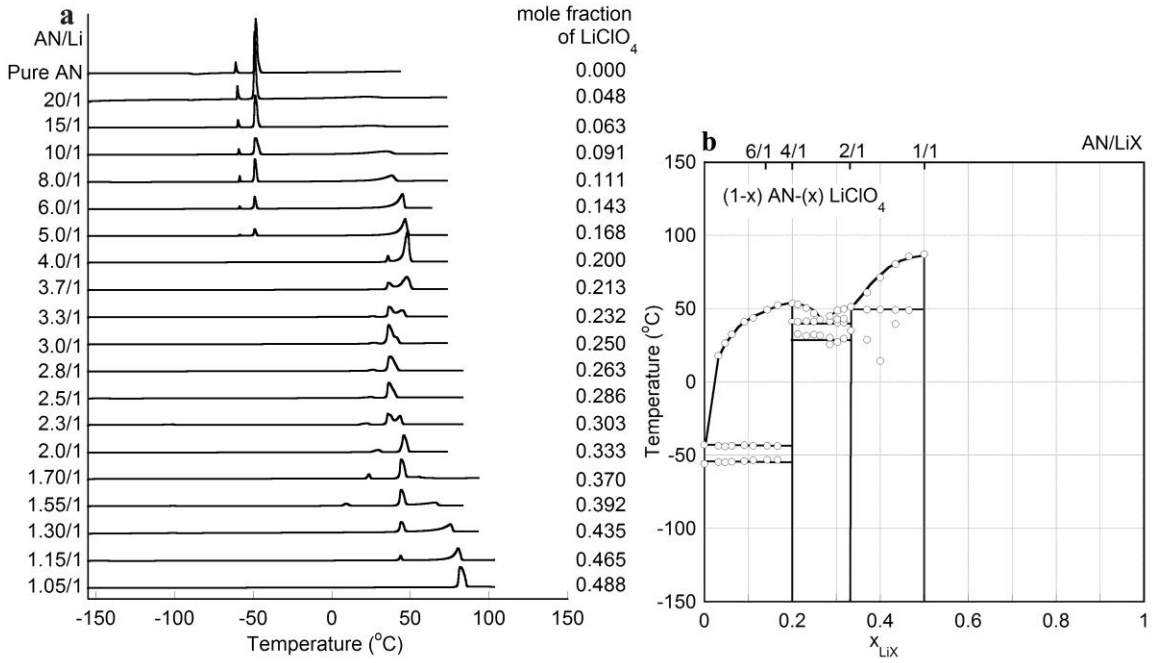

Figure 1-9. (a) DSC plot and (b) phase diagram of $(AN)_n$-$LiClO_4$ mixtures.[61]

phase diagram. The straight vertical lines in the phase diagram give the compositions of the different solvates present. Once the solvate compositions are known from the phase diagram, single crystal solvate structures, where available, are solved using x-ray diffraction. The known solvate structures provide direct information regarding the coordination of Li^+ cations with the solvents and the anions.[56,57]

Raman spectroscopy is an excellent tool for identifying the kind of solvate species (SSIPs, CIPs or AGGs) present in the mixtures since the anion and solvent vibrational bands are sensitive to changes in Li^+ cation coordination.[58-63] The Raman spectra, in conjunction with the crystalline solvate structures, have been used to unambiguously assign the Raman bands to specific forms of anion coordination to Li^+ cations. Once the different crystalline solvates

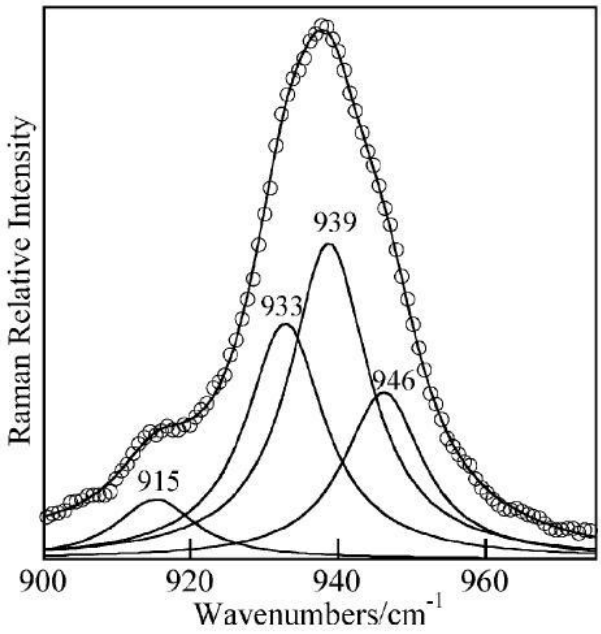

Figure 1-10. Raman spectral analysis of solvate structures in a $(G4)_n$-$LiClO_4$ (n = 0.5) solution.[60]

(SSIPs, CIPs, AGGs) were characterized, the spectroscopic information was applied to understand the molecular-level interactions occurring in the liquid phase. For example, Lassègues *et al.* studied the various crystalline solvate structures formed between $LiClO_4$ and glymes and assigned Raman spectra for SSIP, CIP and AGG solvates containing the ClO_4^- anion at room temperature.[64] They then used these Raman bands to analyze the Raman spectra for tetraglyme $(G4)_n$-$LiClO_4$ (n = 0.5) liquid mixture at 70°C.[64] The broad Raman band, shown in Figure 1-10, for the ClO_4^- anion vibration in the υ_1 range (υ_1 is the symmetric stretching band which is particularly useful for studying $Li^+ \ldots ClO_4^-$ interactions in $LiClO_4$ solvates) is deconvoluted into peaks at 933, 939 and 946 cm^{-1} corresponding to SSIP, CIP

and AGG solvates, respectively. From the relative areas of the peaks, the fraction of different solvates in the liquid mixtures was calculated.[54] Thus, tremendous insight is gained by characterizing the crystalline solvates first and then using this information as a guide to understand the complex interactions occurring in liquid electrolytes.

References

(1) Xu, K. Nonaqueous liquid electrolytes for lithium-based rechargeable batteries. *Chem. Rev*. **2004**, *104*, 4303.

(2) Linden, D.; Reddy, T. B. *Handbook of Batteries*. 3rd ed.; McGraw-Hill: New York, **2001**.

(3) Dudley, J. T.; Wilkinson, D. P.; Thomas, G.; LeVae, R.; Woo, S.; Blom, H.; Horvath, C.; Juzkow, M. W.; Denis, B.; Juric, P.; Aghakian, P.; Dahn, J. R. Conductivity of electrolytes for rechargeable lithium batteries. *J. Power Sources* **1991**, *35*, 59.

(4) Klassen, B.; Aroca, R.; Nazri, M.; Nazri, G. A. Raman spectra and transport properties of lithium perchlorate in ethylene carbonate based binary solvent systems for lithium batteries. *J. Phys. Chem. B* **1998**, *102*, 4795.

(5) Ding, M. S.; Xu, K.; Jow, T. R. Liquid-solid phase diagrams of binary carbonates for lithium batteries. *J. Electrochem. Soc.* **2000**, *147*, 1688.

(6) Reichardt, C. *Solvents and Solvent Effects in Organic Chemistry*. 3rd ed.; Wiley-VCH: Weinheim, **2005**.

(7) James, D. W.; Mayes, R. E. Ion-ion-solvent interactions in solution. 8. Spectroscopic studies of the lithium perchlorate/*N*,*N*-dimethylformamide system. *J. Phys. Chem.* **1984**, *88*, 637.

(8) James, D. W.; Mayes, R. E. Ion-ion-solvent interactions in solution. I. Solution of $LiClO_4$ in acetone. *Aust. J. Chem.* **1982**, *35*, 1785.

(9) Arora, P.; Zhang, Z. Battery separators. *Chem. Rev.* **2004**, *104*, 4419.

(10) Whittingham, M. S. Electrical energy storage and intercalation chemistry. *Science* **1976,** *192*, 1126.

(11) Whittingham, M. S. Chemistry of intercalation compounds: Metal guests in chalcogenide hosts. *Prog. Solid State Chem.* **1978**, *12*, 41.

(12) Mizushima, K.; Jones, P. C.; Wiseman, P. J.; Goodenough, J. B. Li_xCoO_2 ($0 < x < 1$): A new cathode material for batteries of high energy density. *Mater. Res. Bull.* **1980**, *15*, 783.

(13) Murphy, D. W.; Christian, P. Solid state electrodes for high energy batteries. *Science* **1979**, *205*, 651.

(14) Von Sacken, U.; Nodwell, E.; Sundler, A.; Dahn, J. R. Comparative thermal stability of carbon intercalation anodes and lithium metal anodes for rechargeable lithium batteries. *Solid State Ionics* **1994**, *69*, 284.

(15) Tobishima, S.I.; Yamaki, J.I. A consideration of lithium cell safety. *J. Power Sources* **1999**, *81*, 882.

(16) Randolph, A. L.; Marcus, J. P.; Esther Sans, T.; Kenneth, J. T. Abuse testing of lithium-ion batteries: Characterization of the overcharge reaction of $LiCoO_2$/graphite Cells. *J. Electrochem. Soc.* **2001**, *148*, A838.

(17) Krause, L. J.; Lamanna, W.; Summerfield, J.; Engle, M.; Korba, G.; Loch, R.; Atanasoski, R. Corrosion of aluminum at high voltages in non-aqueous electrolytes containing perfluoroalkylsulfonyl imides-new lithium salts for lithium-ion cells. *J. Power Sources* **1997**, *68*, 320.

(18) Wang, X.; Yasukawa, E.; Mori, S., Inhibition of anodic corrosion of aluminum current collector on recharging in lithium imide electrolytes. *Electrochimica Acta* **2000**, *45*, 2677.

(19) Plichta, E. J.; Behl, W. K. A low-temperature electrolyte for lithium and lithium-ion batteries. *J. Power Sources* **2000**, *88*, 192.

(20) Nöth, H.; Waldhör, R. The structure of lithiumiodide 3-tetrahydrofuran. *Z. Naturforsch.* **1998**. *53b*, 1525.

(21) Giese, H.-H.; Nöth, H.; Schwenk, H.; Thomas, S. Metal tetrahydridoborates and tetrahydridometallates. Part 22. Structural chemistry of lithium tetrahydroborate ether solvates. *Eur. J. Inorg. Chem.* **1998**, *22*, 941.

(22) Zarges, W.; Marsch, M.; Harms, K.; Koch, W.; Frenking, G.; Boche, G. Crystal structure of α-(trimethylsily1)benzyllithiumtetramethylethylenediamine [C_6H_5CH-($SiMe_3$)LiTMEDA] and α-(phenylthio)benzyllithium - 3 tetrahydrofuran [C_6H_5CH-

(SPh)Li(THF)$_3$] - two benzyllithium compounds with central chirality. *Chem. Ber*. **1991**, *124*, 543.

(23) Cardin, C. J.; Cardin, D. J.; Clegg, W.; Coles, S. J.; Constantine, S. P.; Rowe, J. R.; Teat, S. J. The molecular structure and one-pot synthesis of [Li(thf)$_3$Sn(SiMe$_3$)$_3$]. *J. Organomet. Chem.* **1999**, *573*, 96.

(24) A. Beswick, M.; G. Lawson, Y.; R. Raithby, P.; A. Wood, J.; S. Wright, D. A metallated primary arsine; synthesis and structure of [PhAsHLi$_2$thf]$_\infty$ *J. Chem. Soc., Dalton Trans.* **1999**, *12*, 1921.

(25) Chivers, T.; Downard, A.; Parvez, M. Steric and solvation effects on the aggregation of lithium thioamidates: Single-strand polymers with (LiS)$_n$ and (LiNCS)$_n$ backbones. *Inorg. Chem.* **1999**, *38*, 5565.

(26) Bartlett, R. A.; Olmstead, M. M.; Power, P. P. Structural characterization of the solvate complexes of the lithium diorganophosphides [{Li(Et$_2$O)PPh$_2$}$_\infty$], [{Li(THF)$_2$PPh$_2$}$_\infty$], and [{Li(THF)P(C$_6$H$_{11}$)$_2$}$_\infty$]. *Inorg. Chem.* **1986**, *25*, 1243.

(27) Downard, A.; Nieuwenhuyzen, M.; Seddon, K. R.; van den Berg, J.-A. Structural features of lithium organoborates. *Cryst. Growth Des.* **2002**, *2*, 111.

(28) Kongprakaiwoot, N.; Luck, R. L.; Urnezius, E. Polymeric (diphenylphosphinato)-tetrahydrofuranlithium. *Acta Crystallogr*. **2002**, *E58*, m735.

(29) Henderson, W. A.; Brooks, N. R. Crystals from concentrated glyme mixtures. The single-crystal structure of LiClO$_4$. *Inorg. Chem.* **2003**, *42*, 4522.

(30) Huang, W.; Frech, R.; Wheeler, R. A. Molecular structures and normal vibrations of trifluoromethane sulfonate ($CF_3SO_3^-$) and its lithium ion pairs and aggregates. *J. Phys. Chem.* **1994,** *98*, 100.

(31) Tayebani, M.; Conoci, S.; Feghali, K.; Gambarotta, S.; Yap, G. P. A. Tri- and tetravalent and mixed-valence niobium complexes supported by a tripodal tripyrrolylmethane trianion. *Organometallics* **2000,** *19*, 4568.

(32) Bock, H.; Ansari, M.; Nagel, N.; Claridge, R. F. C. Interactions in crystals CX. The structure of 9,10-bis(diisopropylsilyl) anthracene and of its "naked" radical anion. *J. Organomet. Chem.* **1996**, *521*, 51.

(33) Habereder, T.; Nöth, H. Synthesis and structures of some trisorganylstannyl boranes and triorganylstannyl borates *Z. Anorg. Allg. Chem.* **2001**, *627*, 789.

(34) Link, H.; Decker, A.; Fenske, D. Imido-bridged iron clusters with heterocubane-type structure. The crystal structures of $[Li(THF)_4][Li(THF)_3][Fe_4(\mu_3\text{-}NPh)_4Cl_4]$, $[Li(DME)_3][Fe_4(\mu_3\text{-}NtBu)_4Cl_4]$, $[Fe_4(\mu_3\text{-}NtBu)_4Cl_4] \cdot Et_3PNtBu$, $[Li(THF)_4][Fe_4(NHtBu)_4(\mu_3\text{-}NtBu)_4]$, $_{\infty 1}\{[Li(THF)_2]_2[Fe_2(\mu\text{-}NMes)_2Cl_4]\}$ und $[NnBu_4]_2[Fe_2(\mu\text{-}NPh)_2Cl_4]$. *Z. Anorg. Allg. Chem.* **2000**, *626*, 1567.

(35) Hwang, C.-S.; Power, P. P. Synthesis and characterization of the lithium organoargentate salts $[Li(THF)_4][Ag(Triph)_2]THF$ and $[Li(THF)_4][Ag(C_6H_3\text{-}2,6\text{-}Mes_2)_2]_{1/8}\ OEt_2$ (Triph = C_6H_2-2,4,6-Ph_3; Mes = C_6H_2-2,4,6-Me_3). *J. Organomet. Chem.* **1999**, *589*, 234.

(36) Vagedes, D.; Erker, G.; Fröhlich, R. Synthesis and structural characterization of $[H(OEt_2)_2]^+[(C_3H_3N_2)\{B(C_6F_5)_3\}_2]^-$ - a Bronsted acid with an imidazole-derived 'non-coordinating' anion. *J. Organomet. Chem.* **2002**, *641*, 148.

(37) Chan, H.-S.; Yang, Q.; Mak, T. C. W.; Xie, Z. Anionic dichlorolanthanocene compounds. X-ray crystal structures of $[\{(Me_3Si)_2C_5H_3\}_2LnCl_2][Li(THF)_4]$ (Ln=Er, Yb) and $\{(Me_3Si)_2C_5H_3\}_2Yb([\mu]\text{-}Cl)_2Li(THF)_2$. *J. Organomet. Chem.* **2000**, *601*, 160.

(38) Linti, G.; Rodig, A.; Köstler, W. Synthesis and structures of novel triphenylsilyl and triphenylgermyl substituted gallanes and oligogallanes - $[Ga_3(GePh_3)_6]^-$, the first linear trigallane. *Z. Anorg. Allg. Chem.* **2001**, *627*, 1465.

(39) Katritzky, A. R.; Fara, D. C.; Yang, H.; Tämm, K.; Tamm, T.; Karelson, M. Quantitative measures of solvent polarity. *Chem. Rev.* **2004**, *104*, 175.

(40) John, M.; Auel, C.; Behrens, C.; Marsch, M.; Harms, K.; Bosold, F.; Gschwind, R. M.; Rajamohanan, P. R.; Boche, G. The relation between ion pair structures and reactivities of lithium cuprates. *Chem. Eur. J.* **2000**, *6*, 3060.

(41) Hogen-Esch, T. E.; Smid, J. Studies of contact and solvent-separated ion pairs of carbanions. II. Conductivities and thermodynamics of dissociation of fluorenyllithium, sodium, and cesium. *J. Am. Chem. Soc.* **1966**, *88*, 318.

(42) Hope, H.; Olmstead, M. M.; Power, P. P.; Sandell, J.; Xu, X. Isolation and x-ray crystal structures of the mononuclear cuprates $[CuMe_2]^-$, $[CuPh_2]^-$, and $[Cu(Br)CH(SiMe_3)_2]$. *J. Am. Chem. Soc.* **1985**, *107*, 4337.

(43) Shirk, A. E.; Shriver, D. F. Raman and infrared spectra of tetrahydroaluminate, AlH^-, and tetrahydrogallate, GaH^- salts. *J. Am. Chem. Soc* **1973**, *95*, 5904.

(44) Shriver, D. F.; Atkins, P.; Langford, C. H. *Inorganic Chemistry*. 2nd ed.; W. H. Freeman and Company: New York, **1994**.

(45) Firman, P.; Xu, M.; Eyring, E. M.; Petrucci, S. Molecular relaxation dynamics of lithium perchlorate in acyclic polyether solvents. *J. Phys. Chem.* **1993**, *97*, 3606.

(46) Tobishima, S.; Morimoto, H.; Aoki, M.; Saito, Y.; Inose, T.; Fukumoto, T.; Kuryu, T. Glyme-based nonaqueous electrolytes for rechargeable lithium cells. *Electrochim. Acta* **2004**, *49*, 979.

(47) Fujii, K.; Fujimori, T.; Takamuku, T.; Kanzaki, R.; Umebayashi, Y.; Ishiguro, S. I. Conformational equilibrium of bis(trifluoromethanesulfonyl)imide anion of a room-temperature ionic liquid: Raman spectroscopic study and DFT calculations. *J. Phys. Chem. B* **2006**, *110*, 8179.

(48) Xue, L.; Padgett, C. W.; DesMarteau, D. D.; Pennington, W. T. Synthesis and structures of alkali metal salts of bis[(trifluoromethyl)sulfonyl]imide. *Solid State Sci.* **2002**, *4*, 1535.

(49) Henderson, W. A. Glyme Lithium salt phase behavior. *J. Phys. Chem. B* **2006**, *110*, 13177.

(50) Henderson, W. A.; McKenna, F.; Khan, M. A.; Brooks, N. R.; Young, V. G.; Frech, R. Glyme lithium bis(trifluoromethanesulfonyl)imide and glyme-lithium bis(perfluoro-

ethanesulfonyl)imide phase Behavior and solvate structures. *Chem. Mater*. **2005**, *17*, 2284.

(51) Henderson, W. A. Crystallization kinetics of glymes-LiX and PEO-LiX polymer electrolytes. *Macromolecules* **2007**, *40*, 4963.

(52) Henderson, W. A.; Brooks, N. R.; Smyrl, W. H. Polymeric $[Li(NO_3)(monoglyme)]_n$. *Acta Crystallogr.* **2002**, *E58*, m500.

(53) Henderson, W. A.; Passerini, S. Ionic conductivity in crystalline-amorphous polymer electrolytes - $P(EO)_6$:LiX phases. *Electrochem. Commun.* **2003**, *5*, 575.

(54) Grondin, J.; Lassègues, J.-C.; Chami, M.; Servant, L.; Talaga, D.; Henderson, W. A. Raman study of tetraglyme-$LiClO_4$ solvate structures. *Phys. Chem. Chem. Phys.* **2004**, *6*, 4260.

(55) Seo, D. M. *et al.*, unreported data (2008-2009).

(56) Henderson, W. A.; Young, V. G., Jr.; Brooks, N. R.; Smyrl, W. H. Li^+ cation coordination in $[Li_2(CF_3SO_3)_2(diglyme)]$ and $[Li_3(C_2F_3O_2)_3(diglyme)]$. *Acta Crystallogr*. **2002**, *C58*, m501.

(57) Brooks, N. R.; Henderson, W. A.; Smyrl, W. H. Lithium trifluoromethanesulfonate acetonitrile adduct. *Acta Crystallog.* **2002**, *E58*, m176.

(58) Grondin, J.; Lassègues, J.-C.; Chami, M.; Servant, L.; Talaga, D.; Henderson, W. A. Raman study of tetraglyme-$LiClO_4$ solvate structures. *Phys. Chem. Chem. Phys.* **2004**, *6*, 4260.

(59) Stevens, J.; Jacobsson, P. A comparison of acetone and poly(propylene glycol) as solvents for lithium triflate and lithium perchlorate. *Can. J. Chem.* **1991**, *69*, 1980.

(60) Huang, W.; Frech, R.; Wheeler, R. A. Molecular structures and normal vibrations of trifluoromethane sulfonate ($CF_3SO_3^-$) and its lithium ion pairs and aggregates. *J. Phys. Chem.* **1994**, *98*, 100.

(61) Hu, Y.; Wang, Z.; Li, H.; Huang, X.; Chen, L. Spectroscopic studies on the cation-anion, cation-solvent and anion-solvent interactions in the $LiCF_3SO_3$/acetamide complex system. *Spectrochim. Acta, Part A* **2005**, *61*, 403.

(62) Sanders, R. A.; Frech, R.; Khan, M. A. Structural investigation of crystalline and solution phases in *N,N,N',N'*-tetramethylethylenediamine (TMEDA) with lithiuum triflate ($LiCF_3SO_3$) and sodium triflate ($NaCF_3SO_3$). *J. Phys. Chem. B* **2003**, *107*, 8310.

(63) Alía, J. M.; Edwards, H. G. M. Ion solvation and ion association in lithium trifluoromethanesulfonate solutions in three aprotic solvents. An FT-Raman spectroscopic study. *Vib. Spectrosc.* **2000**, *24*, 185.

(64) Grondin, J.; Talaga, D.; Lassègues, J.-C.; Henderson, W. A. Raman study of crystalline solvates between glymes $CH_3(OCH_2CH_2)OCH_3$ (n = 1, 2 and 3) and $LiClO_4$. *Phys. Chem. Chem. Phys.* **2004**, *6*, 938.

Chapter 2. Experimental

2.1 Materials

Anhydrous $LiClO_4$ (battery grade, 99.99 %) was purchased from Sigma-Aldrich and used as-received. Diethyl carbonate, (DEC, anhydrous, ≥ 99%), dimethyl carbonate, (DMC, anhydrous, ≥ 99%), methyl acetate (MA, anhydrous, ≥ 99.8%), ethyl acetate (EA, anhydrous, ≥ 99.8%), monoglyme (G1, anhydrous, 99.5%), diglyme (G2, anhydrous, 99.5%), triglyme (G3, anhydrous, 99%), 12-crown-4 (12C4, anhydrous, ≥ 98%), acetonitrile (AN, anhydrous, 99.8%), 2,9-dimethyl-1,10-phenanthroline (DMP, crystalline), ethylene carbonate (EC, anhydrous, 99%), *N,N,N',N'',N''*-pentamethyldiethylenetriamine (PMDETA, anhydrous, 99%), 2-methylpyridine (2-MPY, purum, ≥ 98%) and γ-butyrolactone (GBL, anhydrous, ≥ 98%) were also purchased from Sigma-Aldrich and used as-received. They were handled and stored in an inert atmosphere (N_2) glove box (< 5 ppm H_2O).

2.2 Sample Preparation

For the study of linear carbonates and carboxylic esters with $LiClO_4$ (discussed in Chapter 4), samples were prepared in an inert atmosphere (N_2) glove box (< 5 ppm H_2O) and stored in hermetically sealed glass vials. The crystalline solvates, discussed in Chapter 3, were prepared using two different methods. The solvates whose structures are already known were prepared by mixing the stoichiometric amount of solvent and salt in small vials in the glove box. The samples were then heated on a hot plate and stirred with a magnetic stirrer to make homogeneous solutions. The white powders that formed (the solvates have a melting point

(T_m) higher than room temperature) were then transferred to a Linkam stage (the Linkam stage is a temperature controlled stage which hermetically seals the sample) for Raman analysis or to DSC pans for thermal characterization. For the solvates with unknown crystal structures, single crystals were grown. From the phase diagram, the probable solvates were identified. Then slightly more dilute solutions were made and stored at an appropriate temperature (identified using a phase diagram, where available) to form single crystals. In some cases, solvates for other salts were identified from the literature and the same solvent was used to grow single crystals.

2.3 Thermal Characterization: Differential Scanning Calorimetry

Thermal measurements were carried out using a TA Instruments Q2000 differential scanning calorimeter (DSC) with liquid nitrogen cooling. Hermetically sealed aluminium pans were prepared in the glove box. Typically, for the Raman characterization of ClO_4^- solvates (discussed in Chapter 3), the sample pans were cooled to -150°C and then heated to 100°C at 5°C min^{-1} to get the melting peak for the solvates. Also, for the study of linear carbonates and carboxylic esters with $LiClO_4$ (discussed in Chapter 4), the sample pans were cooled to -150°C and then heated to 100°C at 5°C min^{-1} in the final run. In most of the cases, it was necessary to hold or cycle the samples at various subambient temperatures before the final measurement to ensure complete crystallization. The DSC data were used to get the T_m of the phases present, as well as the glass transition (T_g) if the solutions remained amorphous. From this information, the phase diagrams were prepared.

2.4 Raman Measurements

A Horiba Jobin-Yvon LabRam HR Vis confocal Raman spectrometer was used for the spectroscopic analysis. This instrument is equipped with a HeNe laser (633 nm), an air-cooled CCD detector and a 1800 grooves mm^{-1} grating. Before the measurements, the spectrometer was calibrated with the silicon band at 520.7 cm^{-1}. Measurements were performed with an LTS350 Linkam heating/cooling stage and a long distance 50X optical objective. The samples were hermetically sealed in the Linkam stage in the glove box and the temperature of the samples was controlled with liquid N_2. For the Raman characterization of the ClO_4^- solvates (Chapter 3), spectra were typically collected using a 10 s measurement time and five accumulations. The samples were cooled/heated at 20°C min^{-1} and the spectra were collected from -100°C to 60°C at an interval of 20°C. For the study of linear carbonates and carboxylic esters with $LiClO_4$ (Chapter 4), the samples were crystallized in the Linkam stage following the same procedure used in the DSC analysis before collecting the Raman spectra for the solid mixtures. The Raman spectra of the liquid mixtures were also collected. The spectra were measured and analyzed using LabSpec Software to determine the anion vibration band positions, as well as band deconvolution and area integration.

2.5 Solvate Crystal Structure Determination: X-ray Diffraction

The single crystal structures of the solvates were solved using x-ray diffraction. The samples were mounted on a nylon loop with a small amount of Paratone N oil. All X-ray

measurements were made on a Bruker-Nonius Kappa Axis X8 Apex2 diffractometer. The unit cell dimensions were determined from a symmetry constrained fit of the reflections and angles. The data collection strategy was a number of ω and φ scans. The frame integration was performed using SAINT.[1] The resulting raw data were scaled and absorption corrected using a multi-scan averaging of symmetry equivalent data using SADABS.[2] The structures were solved by direct methods using the XS program.[3] The structural models were fit to the data using a full matrix least-squares method. The structures were refined using the XL program from SHELXTL.[3] Graphic plots of the structures were produced using Mercury 2.4 software. This work was carried out by Dr. Paul Boyle in the Department of Chemistry, North Carolina State University.

References

(1) SAINT *version* 2008.6; Bruker-Nonius: Madison, WI, USA, **2008**.

(2) SADABS *version* 2008.4; Bruker-Nonius: Madison, WI, USA, **2009**.

(3) Bruker-AXS, XS *version* 2009.9, Bruker-AXS, Madison, WI, USA, **2009**.

Chapter 3. Raman Characterization of $Li^+...ClO_4^-$ Coordination

3.1 Introduction

Raman spectra can be used to identify the kind of solvates (SSIPs, CIPs and AGGs) present in the aprotic solvent-LiX mixtures. When an anion is coordinated to one or more Li^+ cations, the electron cloud distribution, bond lengths and symmetry change, which leads to changes in the anion vibrational bands. Raman bands for electrolyte liquid mixtures, however, are difficult to interpret because of the presence of a number of different, often overlapping, vibrational bands present from the various solvates. The complex equilibria between the different solvates in the liquid state can only be reasonably estimated if the spectra for the particular solvates can be accurately assigned. In the present study, $LiClO_4$ solvates with known crystal structures have been characterized to unambiguously assign the Raman bands to specific forms of ClO_4^- coordination to Li^+ cations. $LiClO_4$, although not useful for commercial electrolyte applications because of its powerful oxidizing properties,[1-3] is quite useful for understanding ion solvation using spectroscopic studies.[4] ClO_4^- anions have a tetrahedral symmetry[5,6] and show significant geometrical and spectral changes when they are coordinated by metal ions such as Li^+ cations.[7] Lassègues *et al*. utilized the known crystalline solvate structures of glymes with $LiClO_4$[8,9] and the structure of pure $LiClO_4$ salt[5,6] to establish vibrational assignments for the ClO_4^- anion with SSIP, CIP-I, CIP-II, AGG-I and AGG-III coordination. The present study is a more extensive investigation which examines numerous ClO_4^- solvates, in addition to the glyme-$LiClO_4$ solvates, to confirm the Raman bands for specific forms of ClO_4^- coordination to Li^+ cations. In addition, for the first time,

AGG-II solvates (ClO_4^- anion coordinated to three Li^+ cations) have been characterized. Unlike Lassègues *et al.* who assigned the Raman bands only at room temperature, this study also focused on the effect of temperature on the anion vibration bands by collecting the Raman spectra of the solvates over a wide temperature range (-100 to 60°C).

3.2 Solvates Studied: Structural and Thermal Data

In the present study, thirteen different solvates, along with pure $LiClO_4$, have been characterized with Raman spectroscopy. The structures of some of the solvates were known prior to the present study. Crystal structures of five new solvates—$(EC)_3$:$LiClO_4$, $(PMDETA)_1$:$LiClO_4$, $(GBL)_1$:$LiClO_4$, $(DEC)_1$:$LiClO_4$ and $(EA)_1$:$LiClO_4$—have been determined for this study. Figure 3-1 gives the structures of the various solvents used for making the solvates and Table 3-1 gives the geometrical parameters of the solvates studied. Li^+ cation coordination for the different solvate structures is given in Figure 3-2 and the DSC heating traces for the solvates are given in Figure 3-3.

SSIPs

The four SSIPs characterized with Raman are $(G2)_2$:$LiClO_4$, $(12C4)_{3/2}$:$LiClO_4$, $(AN)_4$:$LiClO_4$ and $(DMP)_2$:$LiClO_4$:MeOH.

***$(G2)_2$:$LiClO_4$*:** The $(G2)_2$:$LiClO_4$ SSIP solvate has an orthorhombic structure with the Li^+ cations coordinated by six ether oxygens from two diglyme (G2) molecules.[8] Since the cations are fully solvated by the solvent molecules and are not coordinated to the anions,

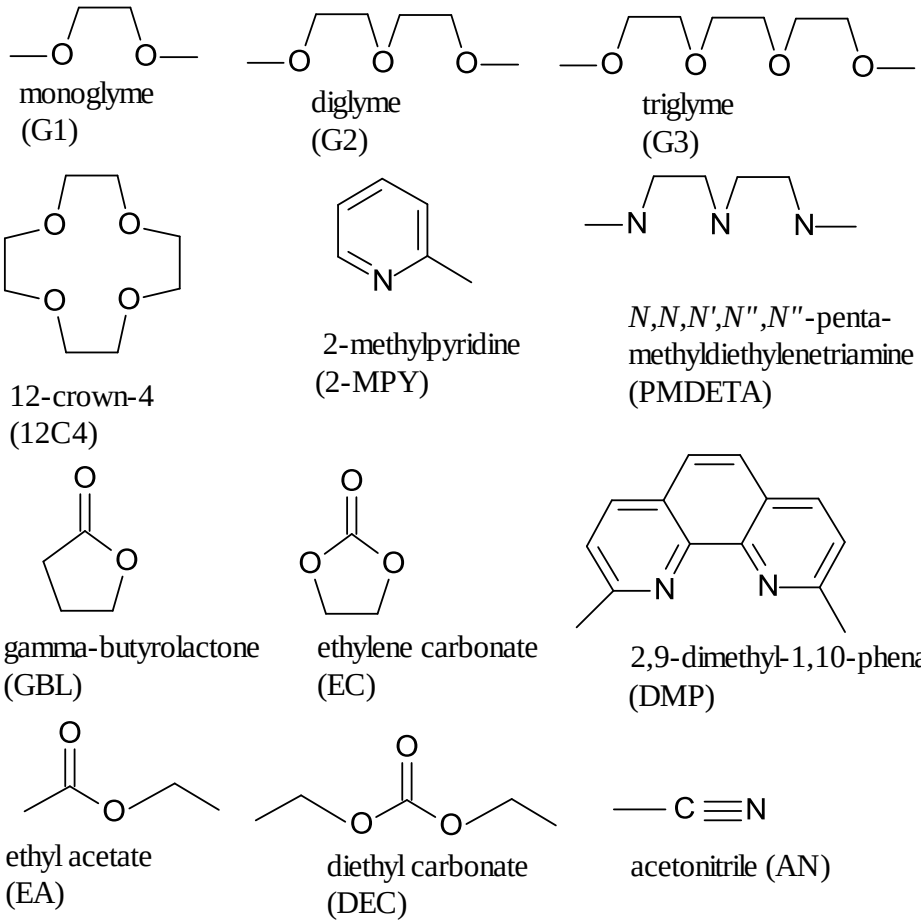

Figure 3-1. Structures of the various solvents used for making the solvates.

$(G2)_2$:$LiClO_4$ forms a SSIP solvate. Two anions, which are ordered and disordered, coexist in the structure. The O-Cl-O angles show that the anions have a slightly distorted tetrahedral geometry with each anion having two shorter and two longer Cl-O bonds. The DSC heating trace of this solvate shows a small solid-solid phase transition around -67°C (this may be due to the order/disorder transition of the anion) and a T_m at around 70°C which matches with the previously reported data.[9]

Table. 3-1. Geometric parameters of the various solvates.

Complex (SSIPs)	Cl-O distances/Å	O-Cl-O angles/°
$(G2)_2$:$LiClO_4$	1.416, 1.418, 1.432, 1.434 1.400, 1.410, 1.452, 1.462	108.92-110.63 107.60-112.30
$(DMP)_2$:$LiClO_4$	1.405, 1.422, 1.384, 1.420	108.30-112.90
$(12C4)_{3/2}$:$LiClO_4$	1.441, 1.434, 1.445, 1.430	108.50-110.20
$(AN)_4$:$LiClO_4$	1.425, 1.442, 1.437, 1.415 1.421, 1.428, 1.402, 1.432 1.407, 1.438, 1.383, 1.399	107.80-111.20 108.50-110.20 107.40-110.80
$(EC)_3$:$LiClO_4$	1.454, 1.435, 1.431, 1.428 1.432, 1.423, 1.436, 1.400	108.58-110.9 107.70-111.70
$(G3)_1$:$LiClO_4$	1.420, 1.423, 1.425, 1.458	108.60-110.10
$(G1)_2$:$LiClO_4$	1.429, 1.429, 1.443, 1.443	106.11-110.46
$(PMDETA)_1$:$LiClO_4$	1.4369, 1.4487, 1.4351, 1.4340	108.59-110.52
$(2\text{-}MPY)_2$:$LiClO_4$	1.4434, 1.4533, 1.4243, 1.4296	107.68-111.70
$(GBL)_1$:$LiClO_4$	1.4505, 1.4576, 1.4244, 1.4272	107.58-110.96
$(DEC)_1$:$LiClO_4$	1.4420, 1.4430, 1.4420, 1.4050	108.10-110.40
$(EA)_1$:$LiClO_4$	1.4456, 1.4412, 1.4436, 1.4188	107.97-110.60

***$(12C4)_{3/2}$:$LiClO_4$*:** In the $(12C4)_{3/2}$:$LiClO_4$ SSIP solvate, one 12C4 molecule lies between two Li^+ cations each of which are coordinated by four oxygen molecules from a peripheral 12C4 and one oxygen from the central 12C4.[10] The two Li^+ cations are thus 'caged' by the solvent molecules, while the anion is uncomplexed. The Cl-O distances of the anion are almost the same showing that the bonds are equal. The DSC data show one peak at -70°C, a very small peak at 16°C and another peak at 145°C. The endothermic peaks at -70 and 16°C may be due to low energy solid-solid phase transitions that occur for this solvate and the peak at 145°C is the T_m.

***$(AN)_4$:$LiClO_4$*:** The $(AN)_4$:$LiClO_4$ SSIP solvate has three different $[Li(CH_3CN)_4]^+$ and ClO_4^- ions in its asymmetric unit. The Li^+ cations are tetrahedrally coordinated by four

CH_3CN molecules and the anions are uncoordinated.[11] The Cl-O distances of the three anions are not equal—one of the anions has Cl-O distances significantly shorter than the others. The T_m of this solvate is 53°C with a small solid-solid phase transition at 41°C.

***$(DMP)_2$:$LiClO_4$:MeOH*:** The $(DMP)_2$:$LiClO_4$:MeOH SSIP solvate adopts a monoclinic structure.[12] The cation, coordinated by the electron lone pairs from the four nitrogen atoms of the two DMP molecules, remains well separated from the uncoordinated anions. The anions are disordered and the wide range of O-Cl-O angles indicates that they are significantly distorted relative to the original tetrahedral structure. The structure also contains methanol since methanol was used to form the crystals. The hydroxyl group of the methanol forms a hydrogen bond with the anion oxygen. The T_m of this solvate is 153°C.

CIPs

***$(G3)_1$:$LiClO_4$:** In the $(G3)_1$:$LiClO_4$ CIP-I solvate, each Li^+ cation is coordinated by four ether oxygens with two from two different G3 molecules and one oxygen atom from the ClO_4^- anion, forming a CIP-I solvate.[13] The G3 molecules are coordinated to two different Li^+ cations, forming linear polymeric chains. The anion is disordered and the Cl-O bond

Figure 3-2. Li^+ cation coordination in crystalline solvate structures: (a) $(G2)_2$:$LiClO_4$,, (b) $(12C4)_{3/2}$:$LiClO_4$, (c) $(AN)_4$:$LiClO_4$, (d) $(DMP)_2$:$LiClO_4$:MeOH, (e) $(G3)_1$:$LiClO_4$, (f) $(EC)_3$:$LiClO_4$, (g) $(G1)_2$:$LiClO_4$, (h) $(PMDETA)_1$:$LiClO_4$, (i) $(2\text{-}MPY)_2$:$LiClO_4$, (j) $(GBL)_1$:$LiClO_4$, (k) $(DEC)_1$:$LiClO_4$, (l) $(EA)_1$:$LiClO_4$ and (m) $LiClO_4$ (Li-purple, O-red, N-blue, Cl-dark green).[5,6,8-12,13,16]

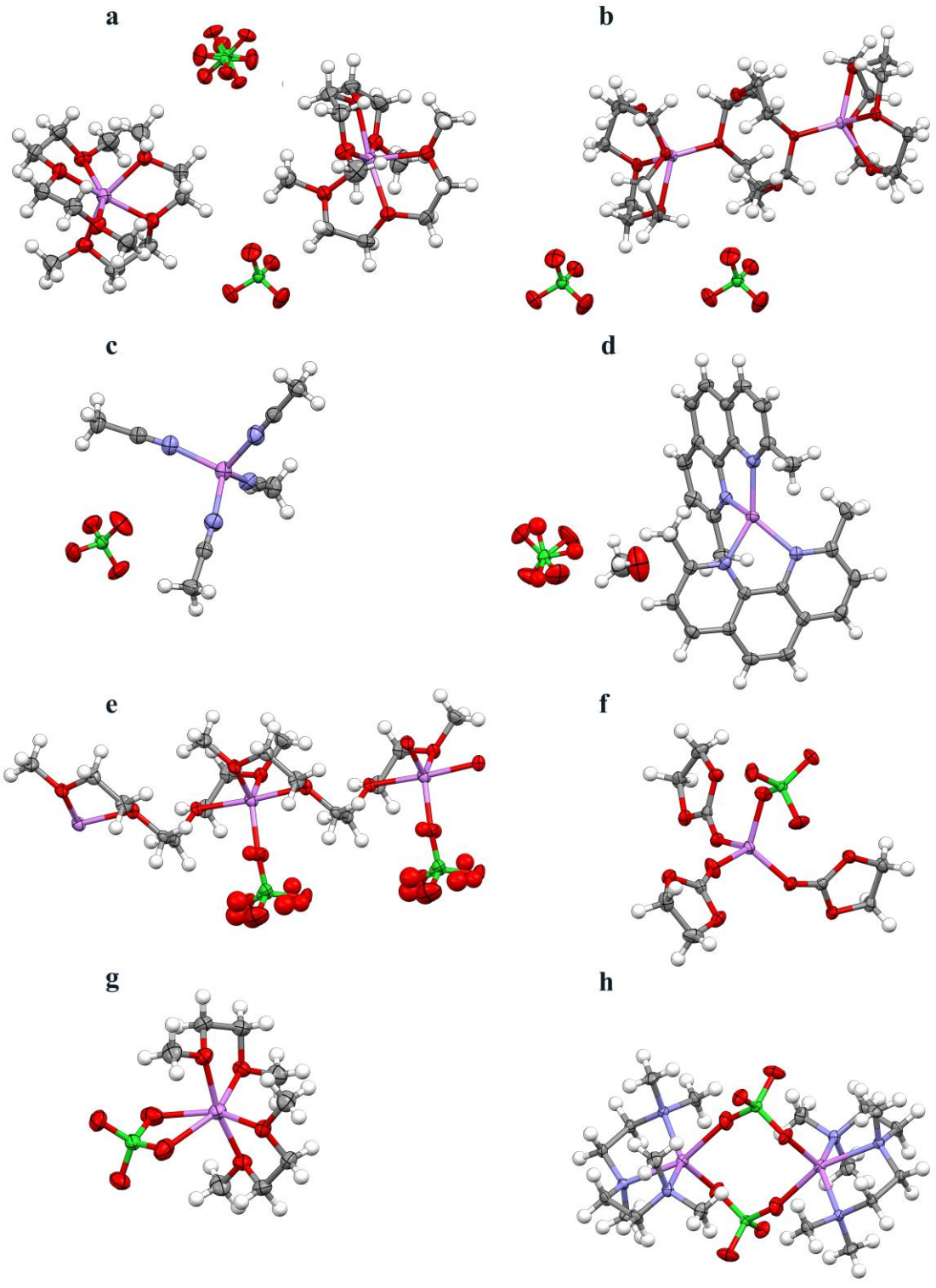
a
b
c
d
e
f
g
h

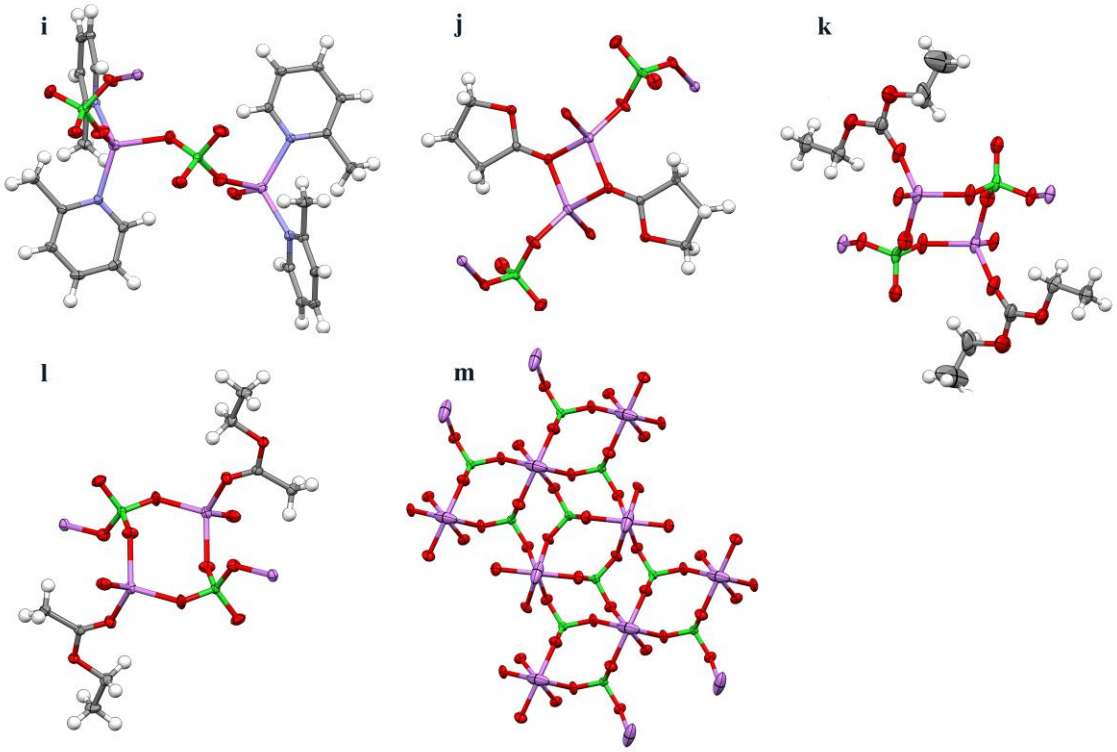

distance for the oxygen coordinating the Li^+ cation is significantly longer than the other Cl-O distances. The T_m of this solvate is 105°C.[9]

$(EC)_3$:$LiClO_4$: The structure of the $(EC)_3$:$LiClO_4$ CIP-I solvates was determined as part of the present work. An $(EC)_n$-$LiClO_4$ (n = 4) mixture at room temperature provided colorless crystals of $(EC)_3$:$LiClO_4$. The crystal structure is a monoclinic structure with the Li^+ cations coordinated by four oxygen molecules, three from three different EC molecules and one from a ClO_4^- anion. Two anions are present in the asymmetric unit with each having one longer Cl-O bond. The T_m of the $(EC)_3$:$LiClO_4$ solvate is 45°C with low energy solid-solid phase transitions at -94°C and 6°C.

***$(G1)_2$:$LiClO_4$*:** The only CIP-II solvate characterized in this study is $(G1)_2$:$LiClO_4$. This solvate consists of Li^+ cations coordinated by four oxygens from two glyme molecules and two oxygens from one ClO_4^- anion, forming a bidentate CIP-II contact ion pair.[8] The Cl-O distances for the oxygens coordinated to the Li^+ cations are longer than for the other Cl-O bonds. The T_m of this solvate is 66°C.[9]

AGG-Is

***$(G2)_1$:$LiClO_4$*:** The structure of the $(G2)_1$:$LiClO_4$ solvate is unknown, but it is speculated to have a AGG-I structure similar to that of $(G2)_1$:$LiCF_3SO_3$[14] and $(G2)_1$:$LiBF_4$.[15] The T_m of this solvate is 81°C.[9]

***$(PMDETA)_1$:$LiClO_4$*:** Colorless crystals of the $(PMDETA)_1$:$LiClO_4$ AGG-I solvates were formed at room temperature from a dilute mixture of $(PMDETA)_n$-$LiClO_4$ (n = 2). The crystal structure confirmed the AGG-I coordination of the solvate. The structure consists of dimers with each Li^+ cation coordinated by the three nitrogen atoms of a PMDETA molecule. Two ClO_4^- anions then join two such solvated cations through the coordination of two oxygen atoms to the two Li^+ cations. The Cl-O distances are almost the same and they have a slightly distorted geometry. The T_m of this solvate is 51°C.

***$(2\text{-}MPY)_2$:$LiClO_4$*:** The $(2\text{-}MPY)_2$:$LiClO_4$ AGG-I solvate has each ClO_4^- anion coordinated to two Li^+ cations forming a linear polymeric structure. The Cl-O distances for the oxygens coordinated to the Li^+ cations are larger than those for the uncoordinated oxygens.[16] The T_m of this solvate is 103°C.

***$(GBL)_1$:$LiClO_4$*:** Colorless crystals of the $(GBL)_1$:$LiClO_4$ AGG-I solvate were formed from a $(GBL)_n$-$LiClO_4$ (n = 1.5) mixture at room temperature. The $(GBL)_1$:$LiClO_4$ solvate also has a dimer structure. Like the $(2\text{-MPY})_2$:$LiClO_4$ solvate, the Cl-O distances for the oxygens coordinated to the Li^+ cations are longer than those for the uncoordinated oxygens. The T_m of this solvate is 103°C.

AGG-IIs

***$(DEC)_1$:$LiClO_4$*:** When a mixture of $(DEC)_n$-$LiClO_4$ (n = 1.52) was held at 35°C, single crystals of the $(DEC)_1$:$LiClO_4$ AGG-II solvate formed. These crystals are stable at room temperature. The $(DEC)_1$:$LiClO_4$ solvate has an highly aggregated structure. Each Li^+ cation coordinated to four oxygen atoms, with one carbonyl oxygen from DEC and three oxygens from three different anions. The anions, in turn, are coordinated to three different Li^+ cations resulting in a polymeric chain. The Cl-O distances for the oxygens coordinated to the Li^+ cations are the same. The Cl-O distances are longer for the uncoordinated oxygens than those for the coordinated oxygens. The T_m of this solvate is 54°C.

***$(EA)_1$:$LiClO_4$*:** Single crystals of the $(EA)_1$:$LiClO_4$ AGG-II solvate were formed by storing a $(EA)_n$-$LiClO_4$ (n = 2) mixture in the refrigerator at approximately 4°C. The structure is very similar to that for the $(DEC)_1$:$LiClO_4$ solvate, but the Cl-O distances for the oxygens coordinated to the Li^+ cations are longer for $(EA)_1$:$LiClO_4$ as compared to $(DEC)_1$:$LiClO_4$. The T_m of this solvate is 34°C.

AGG-III

Pure $LiClO_4$: Pure $LiClO_4$, which has an AGG-III structure, was also characterized for comparison. The ClO_4^- anions have almost perfect tetrahedral symmetry with each anion coordinated to six different Li^+ cations. Among the four anion oxygens, two coordinate a single Li^+ cation each and the remaining two coordinate two cations each.[5,6]

3.3 Results and Discussion

The isolated ClO_4^- anion is tetrahedral in structure with four modes of vibration denoted by υ_1, υ_2, υ_3 and υ_4.[7,17-21] The Raman spectra for the υ_1, υ_2 and υ_4 vibrations of various solvates from -100 to 60°C at intervals of 20°C are given here (Figures 3-4 to 3-9). Since the Raman bands for pure glyme solvents and the solvates overlap strongly in the υ_3 region, Raman spectra for the υ_3 vibration are not reported.

SSIPs

$(G2)_2$:$LiClO_4$: The Raman spectra for the $(G2)_2$:$LiClO_4$ SSIP solvate at -100°C (Figure 3-4) show narrow bands at 459 and 624 cm^{-1} for the υ_2 and υ_4 vibrations, respectively. The small shoulder at 621 cm^{-1} for the υ_4 vibration is due to the isotopic effect of $^{35}Cl/^{37}Cl$.[17] The υ_1 and υ_2 bands are not significantly affected by the presence of the isotope, but the υ_4 vibration is split into two components separated by approximately 3 cm^{-1}.[17] For the υ_1 vibration, at -100°C, the band splits into two bands—one at 932 cm^{-1} and the other at around 934 cm^{-1}. This could be due to the presence of ordered and disordered anions in the $(G2)_2$:$LiClO_4$ structure.[4] Since the sample was cooled rapidly, it may not have undergone the

order/disorder transition, resulting in the splitting of the bands. The weak band at 911 cm^{-1} is due to the $2\upsilon_2$ overtone in the Fermi resonance with the υ_1 vibration of the ClO_4^- anion.[20,22] The wavenumber values agree quite well with the data reported by Lassègues *et al*. and others in the literature.[4,18-21] For all of the modes of vibration, as the temperature increases, the peak wavenumber shifts to lower value.

***$(DMP)_2$:$LiClO_4$:MeOH*:** The $(DMP)_2$:$LiClO_4$:MeOH SSIP solvate has characteristic peaks that match very well with the peaks for the $(G2)_2$:$LiClO_4$ solvate. The extra peaks found in the υ_2 and υ_4 vibration regions are due to the coordination of solvent with the Li^+ cation.[23] For the υ_1 region, a band is present at 934 cm^{-1} with a shoulder at 933 cm^{-1} at a temperature of -100°C. The shoulder may be due to the Li^+ cation coordinating with the solvent.[24] It should be mentioned that even though $(DMP)_2$:$LiClO_4$:MeOH has hydrogen bonding between methanol and the anion, the anion Raman bands are not affected notably by it.

***$(12C4)_{3/2}$:$LiClO_4$*:** The $(12C4)_{3/2}$:$LiClO_4$ SSIP solvate gives a sharp peak at 933 cm^{-1} with a $2\upsilon_2$ overtone at 911 cm^{-1}. The extra band in the υ_2 vibration region at around 490 cm^{-1} could be due to the solvent coordinated to the Li^+ cation.[25]

***$(AN)_4$:$LiClO_4$*:** The $(AN)_4$:$LiClO_4$ SSIP solvate gives peaks at 911, 921, 932, 934, 940 and 950 cm^{-1}. Pure AN has a peak at 920 cm^{-1} (Figure 3-10) and, when AN coordinates with a Li^+ cation, it gives a peak at around 934 cm^{-1}.[26] Thus, there is an overlap between the anion band and the band for the solvent coordinated to the Li^+ cation. This may lead to some error in the analysis.

CIPs

$(G3)_1$:$LiClO_4$: The Raman spectra for the two CIP-I solvates studied are given in Figure 3-5. The $(G3)_1$:$LiClO_4$ solvate gives a peak at 942 cm^{-1} for the υ_1 vibration at -100°C and the peak shifts to lower wavenumber as the temperature increases. For the υ_4 vibration, band splitting is observed giving peaks at 620, 624 and 636 cm^{-1} at -100°C. The band splitting suggests that the anions in the $(G3)_1$:$LiClO_4$ solvate are more distorted from the T_d symmetry as compared to the anions in the $(G2)_2$:$LiClO_4$ solvate. As the temperature increases, the peaks become broader with components at 620 and 634 cm^{-1} at 20°C. The values agree well with the ones reported by Lassègues *et al.* at room temperature.[4] The broadening of the bands may be due to the presence of anions that are disordered over three positions. Splitting of the bands at low temperature is also observed for the υ_2 mode of vibration. Lassègues *et al*. did not observe the band splitting because they collected Raman spectra for the solvate in the υ_2 and υ_4 vibration regions at room temperature only.

$(EC)_3$:$LiClO_4$: As for the $(G3)_1$:$LiClO_4$ solvate, this solvate gives a peak at 942 cm^{-1} at a temperature of -100°C for vibrations in the υ_1 region. The extra peak at 905 cm^{-1} is due to EC coordinating with a Li^+ cation.[27] For the υ_4 vibrations, the bands are slightly shifted at a temperature of -100°C, with peaks at 627, 637 and 639 cm^{-1}. The peaks are broad as compared to those for the $(G3)_1$:$LiClO_4$ solvate. The $(EC)_3$:$LiClO_4$ solvate has two anions in the asymmetric unit with different Cl-O distances and O-Cl-O angles. The differences in geometric parameters for the anions result in changes in the vibrations, which may, in turn, contribute to the broadening of the bands.

***$(G1)_2$:$LiClO_4$*:** The $(G1)_2$:$LiClO_4$ solvate provides the only example for bidentate CIP-II coordination. At -100°C, the υ_1 vibration is observed at 925 cm^{-1}, the υ_2 vibration has two components at 449 and 474 cm^{-1} and the υ_4 vibration has five components at 616, 620, 625, 634 and 638 cm^{-1}. Interestingly, unlike the other solvates, the Raman bands for $(G1)_2$:$LiClO_4$ solvate shift to higher wavenumber as the temperature increases.

AGG-Is

***$(G2)_1$:$LiClO_4$*:** The structure of the $(G2)_1$:$LiClO_4$ solvate is unknown, but it is assumed to adopt a dimer structure (AGG-I) similar to $(G2)_1$:$LiCF_3SO_3$ and $(G2)_1$:$LiBF_4$.[14,15] Chabanel *et al*. reported that concentrated solutions of $LiClO_4$ in aprotic solvent form dimer ($Li_2(ClO_4)_2$) solvates, resulting in υ_1 vibrational bands between 946-948 cm^{-1}.[20,21] The υ_1 vibration for the $(G2)_1$:$LiClO_4$ solvate is at 943 cm^{-1} for -100°C, which is quite close to that reported for the dimers.

***$(PMDETA)_1$:$LiClO_4$*:** The AGG-I structure of the $(G2)_1$:$LiClO_4$ solvate is verified by the close resemblance of its Raman bands with those of the $(PMDETA)_1$:$LiClO_4$ solvate. The $(PMDETA)_1$:$LiClO_4$ solvate has an AGG-I structure and at -100°C it gives an asymmetric peak at 943 cm^{-1}. When PMDETA interacts with a Li^+ cation, it has a band at 935 cm^{-1}.[28] So it is likely that the asymmetric band is a combination of an anion band and the band for the solvent coordinating with the Li^+ cations. For the υ_2 vibration, the bands for the $(PMDETA)_1$:$LiClO_4$ solvate are slightly shifted as compared to the $(G2)_1$:$LiClO_4$ solvate. At

-100°C, the $(G2)_1$:$LiClO_4$ solvate has bands at 423 and 454 cm^{-1}, while the $(PMDETA)_1$:$LiClO_4$ solvate has bands at 458 and 463 cm^{-1}. This may be due to the anion bands overlapping with bands from solvent coordinated to Li^+ cations. For the υ_4 mode, the bands of the $(G2)_1$:$LiClO_4$ solvate at -100°C match quite well with those of the $(PMDETA)_1$:$LiClO_4$ solvate.

$(2\text{-}MPY)_2$:$LiClO_4$: The $(2\text{-}MPY)_2$:$LiClO_4$ solvate is another AGG-I structure studied. At a temperature of -100°C, the υ_1 vibration gives a peak at 944 cm^{-1}. The bands for the υ_2 and υ_4 vibration regions are broad, but the peak values match well with the other AGG-I structures. The reason behind the broadening of the band is not understood.

$(GBL)_1$:$LiClO_4$: For the $(GBL)_1$:$LiClO_4$ solvate, there is a peak at 945 cm^{-1} at -100°C. The peaks for the υ_2 and υ_4 regions are sharper than those for the $(2\text{-}MPY)_2$:$LiClO_4$ solvate.

AGG-IIs

$(DEC)_1$:$LiClO_4$: Even though highly aggregated species were identified in aprotic solvent-$LiClO_4$ mixtures,[20,21,29] crystalline AGG-II perchlorate solvates are characterized for the first time in this study. In the υ_1 region, $(DEC)_1$:$LiClO_4$ has a peak at around 955 cm^{-1} at -100°C. The very small peak at 916 cm^{-1} is probably due to the solvent coordinated to Li^+ cations since pure DEC has a band at 900 cm^{-1}. The υ_2 vibrational mode gives peaks at 467 and 483 cm^{-1} and the υ_4 vibration gives peaks at 626, 634 and 651 cm^{-1}.

$(EA)_1$:$LiClO_4$: Another AGG-II characterized is the $(EA)_1$:$LiClO_4$ solvate. This solvate has peaks that are in very good agreement with those of the $(DEC)_1$:$LiClO_4$ solvate. Pure EA

has bands at 441, 461 and 635 cm^{-1} which fall in the υ_2 and υ_4 vibrational regions of the ClO_4^- anion. The small differences for the peaks in the υ_2 and υ_4 regions may arise from the interaction of Li^+ cations with the solvent.

AGG-III

***Pure $LiClO_4$*:** Pure $LiClO_4$, the only AGG-III structure characterized, has a band at 940 cm^{-1} at -100°C. The value matches quite well with that reported by Leong *et al.* for solid $LiClO_4$ salt.[30] For υ_2, the band splits into four components at 456, 465, 480 and 487 cm^{-1}, while υ_4 bands are noted at 615, 621, 660 and 670 cm^{-1}. At 20°C, the splitting is reduced, with three peaks for the υ_2 vibration and two for the υ_4 vibration.

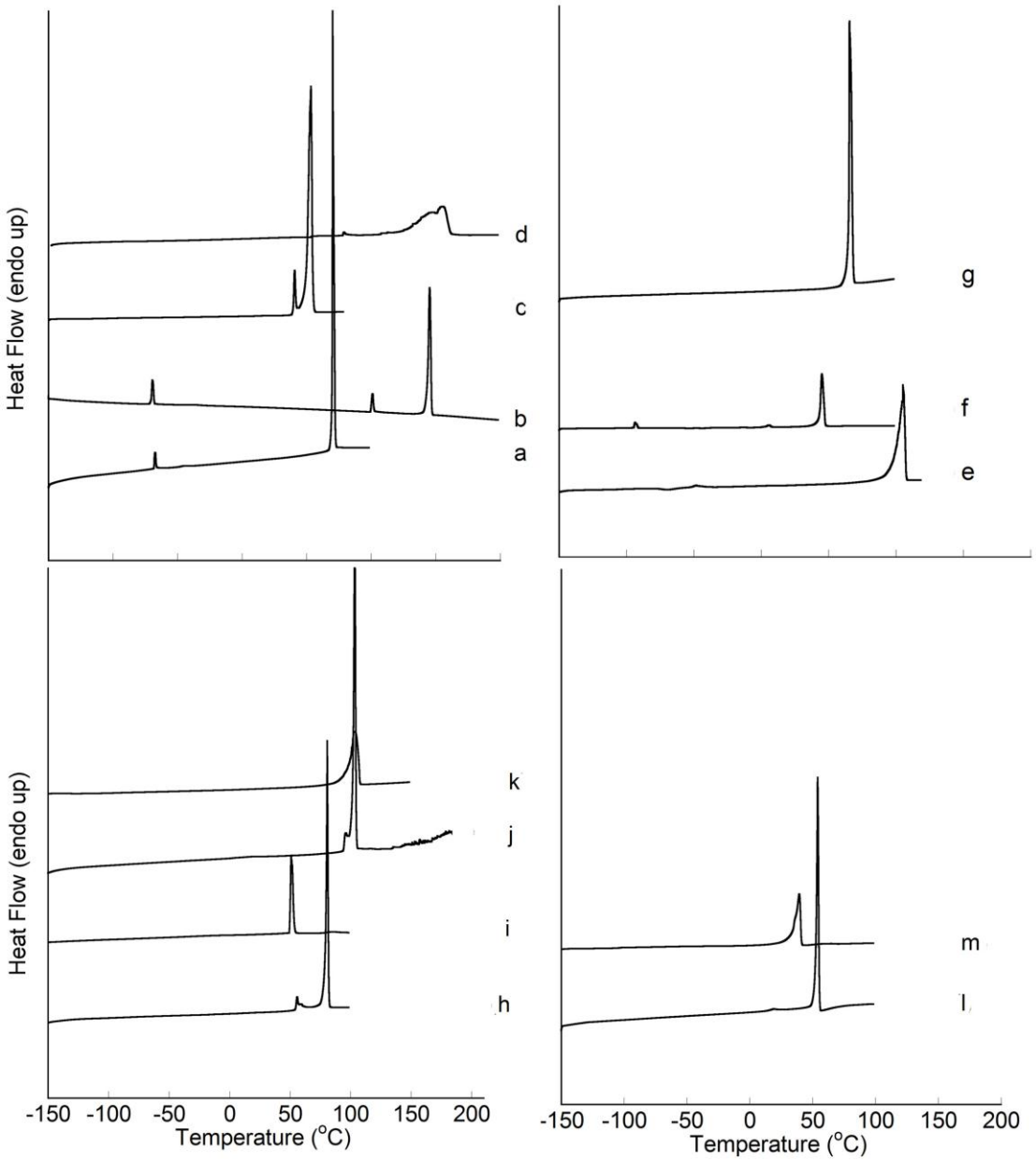

Figure 3-3. DSC heating traces (5°C min^{-1}) of (a) $(G2)_2$:$LiClO_4$, (b) $(12C4)_{3/2}$:$LiClO_4$, (c) $(AN)_4$:$LiClO_4$, (d) $(DMP)_2$:$LiClO_4$, (e) $(G3)_1$:$LiClO_4$, (f) $(EC)_3$:$LiClO_4$, (g) $(G1)_2$:$LiClO_4$, (h) $(G2)_1$:$LiClO_4$, (i) $(PMDETA)_1$:$LiClO_4$, (j) $(2\text{-}MPY)_2$:$LiClO_4$, (k) $(GBL)_1$:$LiClO_4$, (l) $(DEC)_1$:$LiClO_4$ and (m) $(EA)_1$:$LiClO_4$.

Figure 3-4. Raman spectra for υ_2, υ_4 and υ_1 vibrational modes for the ClO_4^- SSIP coordination.

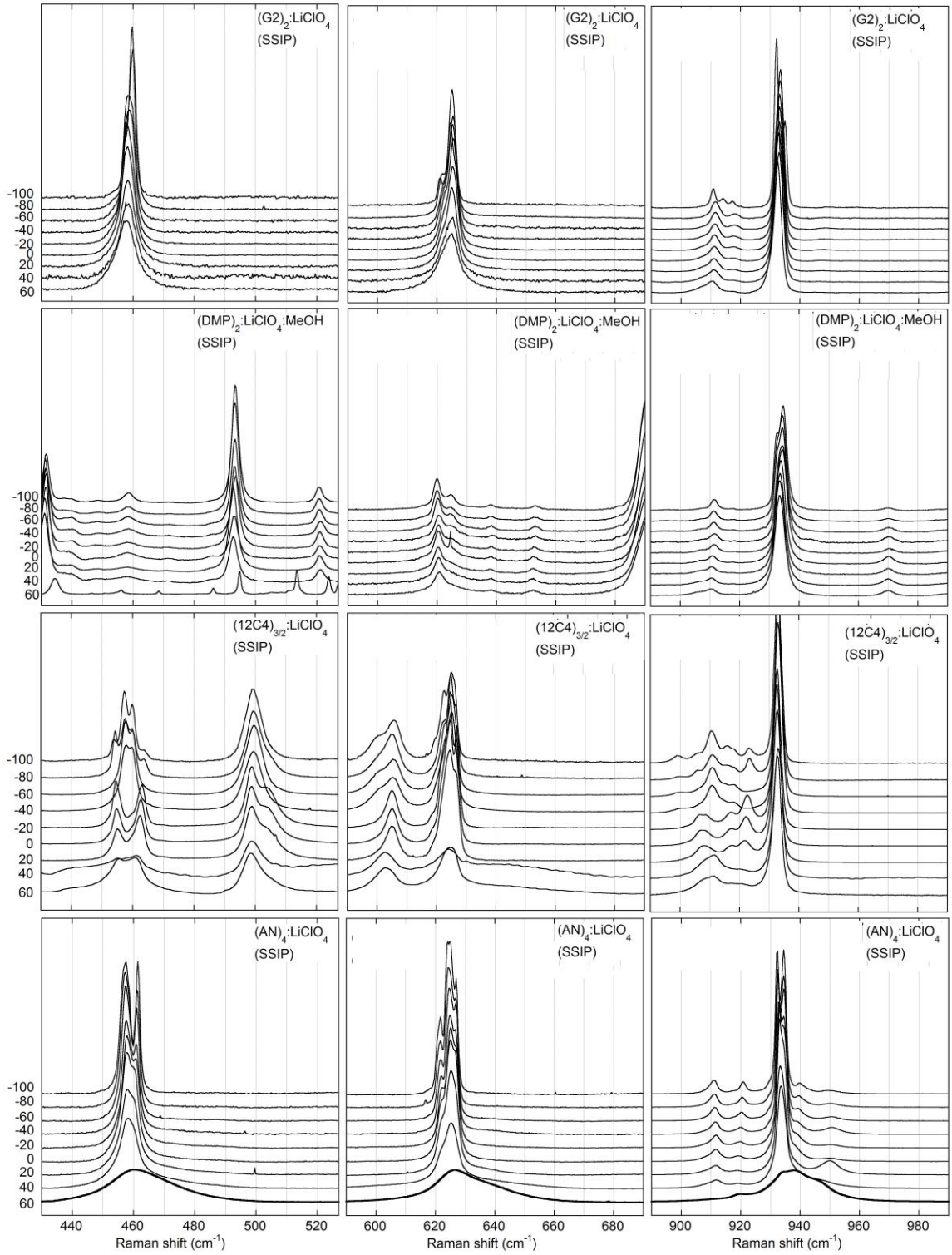
(G2)2:LiClO4 (SSIP)
(DMP)2:LiClO4:MeOH (SSIP)
(12C4)3/2:LiClO4 (SSIP)
(AN)4:LiClO4 (SSIP)
-100
-80
-60
-40
-20
0
20
40
60
440
460
480
500
520
600
620
640
660
680
900
920
940
960
980
Raman shift (cm-1)

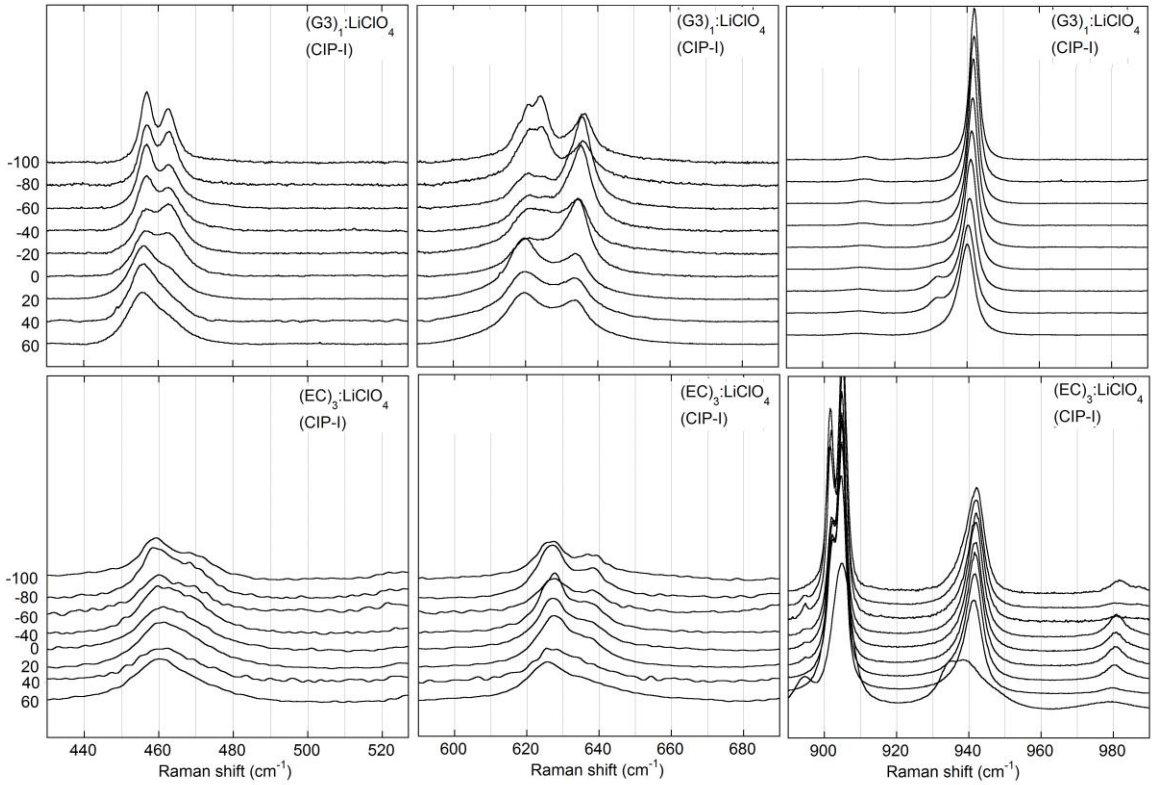

Figure 3-5. Raman spectra for υ_2, υ_4 and υ_1 vibrational modes for the ClO_4^- CIP-I coordination.

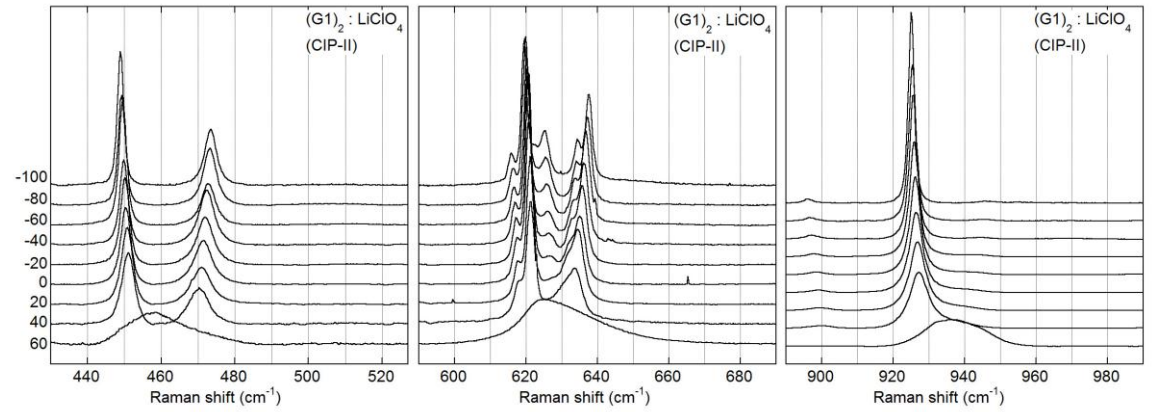

Figure 3-6. Raman spectra for υ_2, υ_4 and υ_1 vibrational modes for the ClO_4^- CIP-II coordination.

Figure 3-7. Raman spectra for υ_2, υ_4 and υ_1 vibrational modes for the ClO_4^- AGG-I coordination.

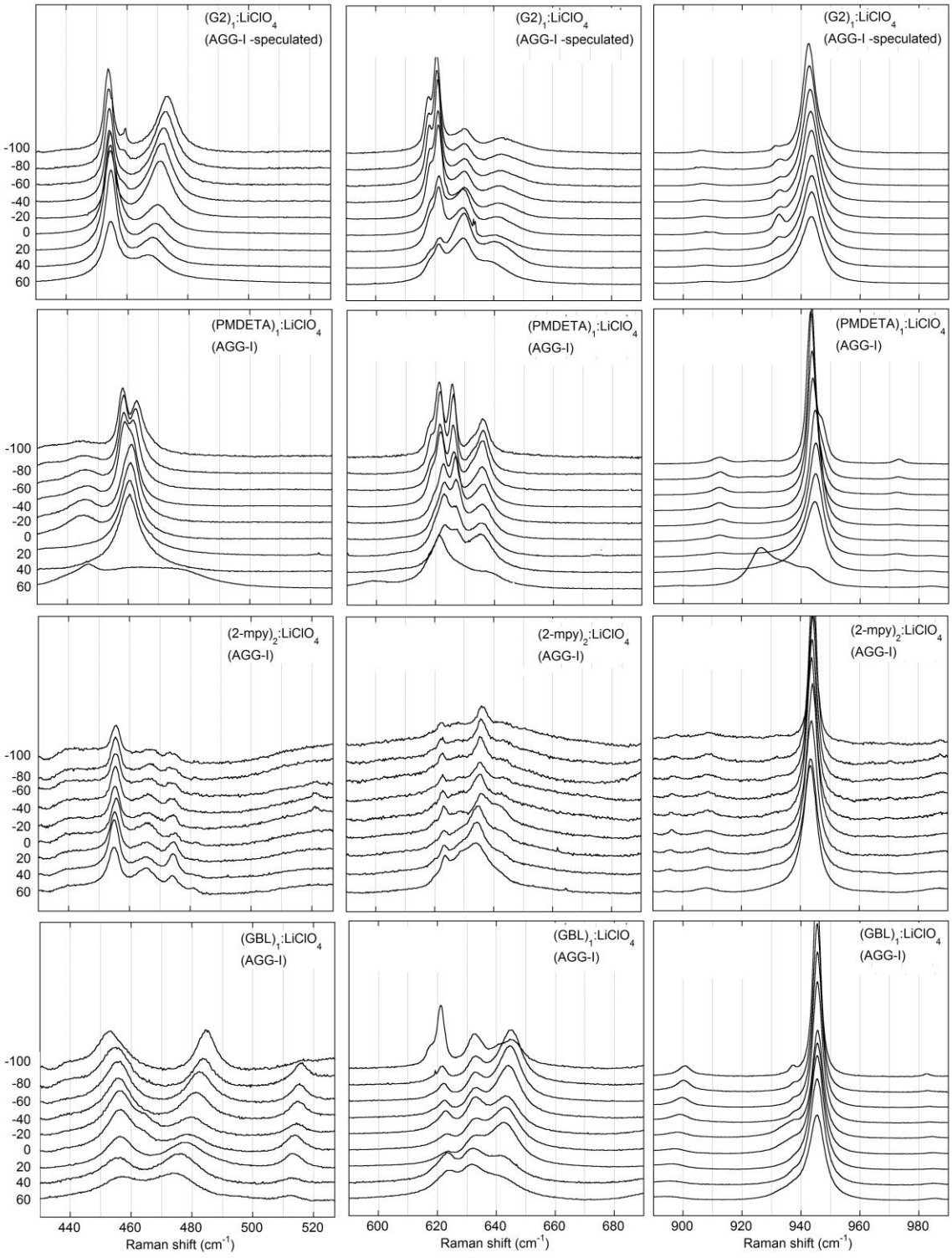
(G2)1:LiClO4
(AGG-I -speculated)
(PMDETA)1:LiClO4
(AGG-I)
(2-mpy)2:LiClO4
(AGG-I)
(GBL)1:LiClO4
(AGG-I)
-100
-80
-60
-40
-20
0
20
40
60
440
460
480
500
520
600
620
640
660
680
900
920
940
960
980
Raman shift (cm-1)

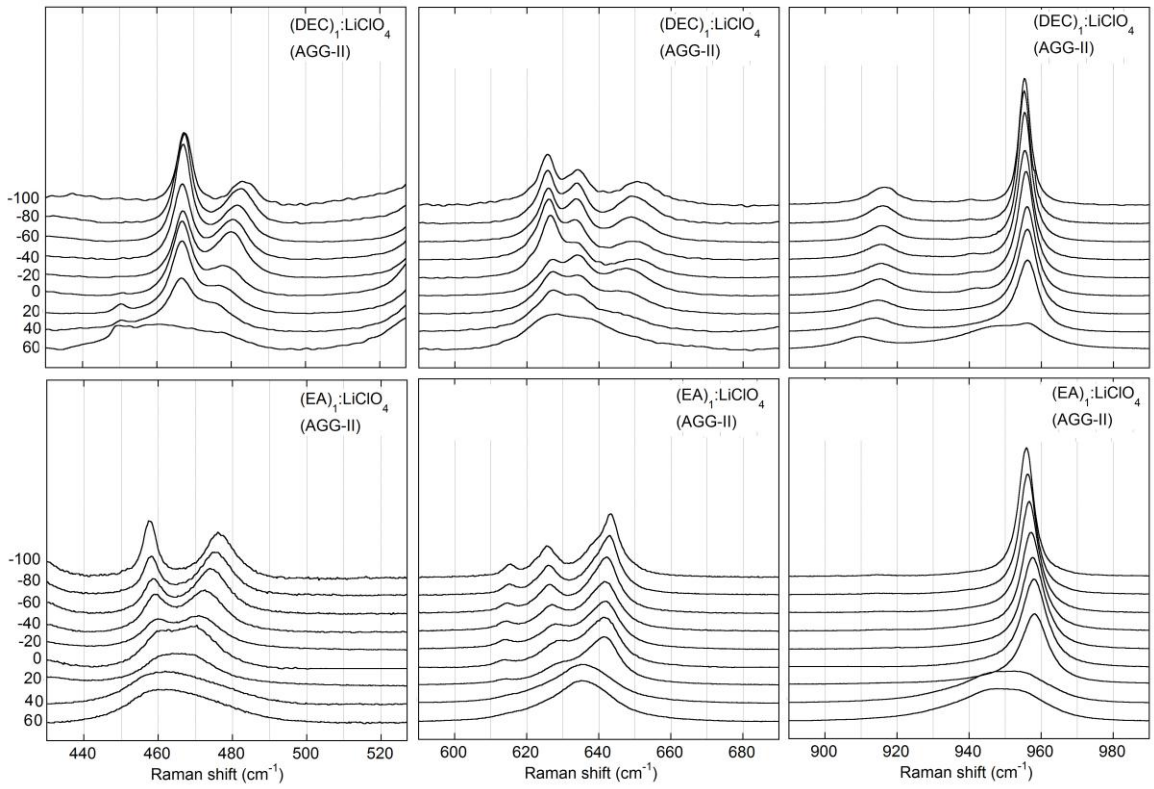

Figure 3-8. Raman spectra for υ_2, υ_4 and υ_1 vibrational modes for the ClO_4^- AGG-II coordination.

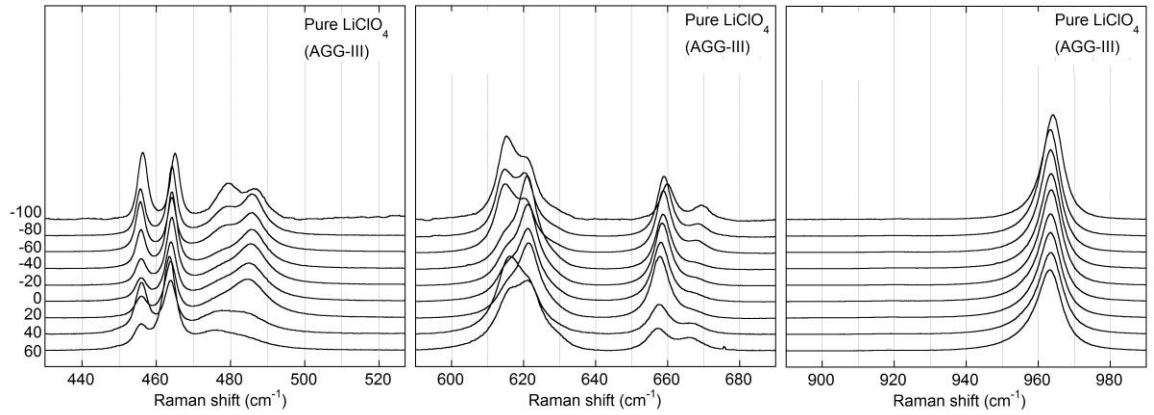

Figure 3-9. Raman spectra for υ_2, υ_4 and υ_1 vibrational modes for the ClO_4^- AGG-III coordination.

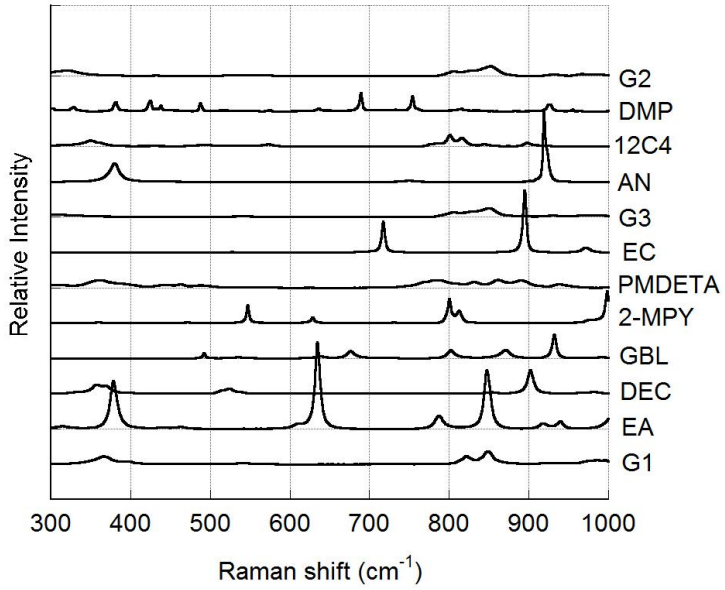

Figure 3-10. Raman bands for the pure solvents.

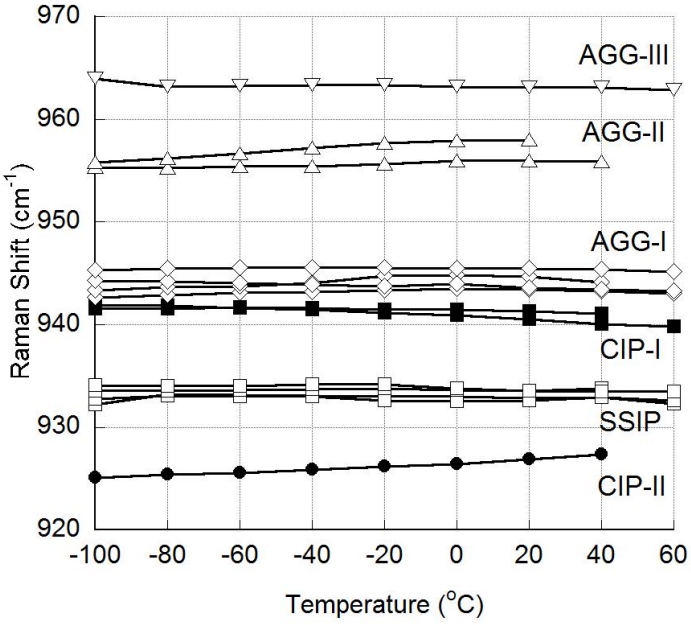

Figure 3-11. Change of the solvate peak positions with temperatures.

3.4 Conclusions

Various ClO_4^- solvates have been characterized to establish the vibrational assignments for ClO_4^- anions involved in different ionic interactions, namely solvent separated ion pairs (SSIP), contact ion pairs (CIP-I, CIP-II), and aggregates (AGG-I, AGG-II, AGG-III). Figure 3-11 summarizes the change of the ClO_4^- anion peak positions with temperature for the different solvates. Even though the solvents differ, the Raman bands, at a particular temperature, are very close for the anions having the same form of coordination with Li^+ cations. From the results, it can be concluded that the υ_1 vibration resulting from the non-degenerate, symmetric stretching band in the 930-965 cm^{-1} region is particularly useful for characterizing $LiClO_4$ solvates. The υ_2 and υ_4 vibration bands are not particularly useful for characterizing the ClO_4^- solvates because of their relatively low intensity and their overlap with the solvent bands. Except for CIP-II solvates, the increase in the number of anions coordinating the Li^+ cations causes the Raman bands to shift to higher wavenumber. On average, for the ClO_4^- anion at -100°C, there are bands at 933, 942, 925, 944, 956 and 964 cm^{-1} corresponding to SSIP, CIP-I, CIP-II, AGG-I, AGG-II and AGG-III solvates, respectively. For the SSIP, CIP-I AGG-I and AGG-III solvates, the peak shifts to slightly lower values as the temperature increases. The peak position for CIP-II and AGG-II solvates, however, moves to higher values with increasing temperature. Further, the Raman bands for CIP-I and AGG-I are positioned close together, leading to some difficulties in differentiatingbetween these two solvates by Raman spectroscopy. For all of the solvates, the

peaks become broader as the temperature increases indicating increased disorder of the ClO_4^- anions with increasing temperature.

References

(1) Xu, K. Nonaqueous liquid electrolytes for lithium-based rechargeable batteries. *Chem. Rev*. **2004**, *104*, 4303.

(2) Newman, G. H.; Francis, R. W.; Gaines, L. H.; Rao, B. M. Hazard investigations of $LiClO_4$ /dioxolane electrolyte. *J. Electrochem. Soc.* **1980**, *127*, 2025.

(3) Jasinski, R.; Carroll, S. Thermal stability of a propylene carbonate electrolyte. *J. Electrochem. Soc.* **1970**, *117*, 218.

(4) Grondin, J.; Lassègues, J.-C.; Chami, M.; Servant, L.; Talaga, D.; Henderson, W. A. Raman study of tetraglyme-$LiClO_4$ solvate structures. *Phys. Chem. Chem. Phys.* **2004**, *6*, 4260.

(5) Wickleder, M. S. Crystal structure of $LiClO_4$. *Z. Anorg. Allg. Chem.* **2003**, *629*, 1466.

(6) Henderson, W. A.; Brooks, N. R. Crystals from concentrated glyme mixtures. The single-crystal structure of $LiClO_4$. *Inorg. Chem.* **2003**, *42*, 4522.

(7) Nakamoto, K. *Infrared and Raman Spectra of Inorganic and Coordination Compounds, Part B*. 5th ed.; Wiley: New York, **1997**.

(8) Henderson, W. A.; Brooks, N. R.; Brennessel, W. W.; Young Jr., V. G. $LiClO_4$ electrolyte solvate structures. *J. Phys. Chem. A* **2003**, *108*, 225.

(9) Henderson, W. A. Glyme-lithium salt phase behavior. *J. Phys. Chem. B* **2006**, *110*, 13177.

(10) Guzei, I. A.; Spencer, L. C.; Xiao, L.; Burnette, R. R. (1,4,7,10-tetraoxacyclododecane)(trideuteroacetonitrile)lithium perchlorate. *Acta Crystallogr.* **2010**, *E66*, m440.

(11) Yokota, Y.; Young Jr., V. G.; Verkade, J. G. The homoleptic lithium complex $[Li(CH_3CN)_4]ClO_4$ *Acta Crystallogr*. **1999**, *C55*, 196.

(12) N., J. H.; Effendya, B.; Mutrofina, S.; Placketta, N. C.; Skeltona, B. W.; Somersa, N.; Whitakera, C. R.; Whitea, A. H. Complexes of group 1 salts with *N*,*N*-aromatic bidentate ligands, of (oligo-/poly-) nuclear or ionic 1:2 salt base ratio. *Z. Anorg. Allg. Chem.* **2006**, *632*, 1839.

(13) Henderson, W. A.; Brooks, N. R.; Brennessel, W. W.; Young Jr., V. G. Triglyme-Li^+ cation solvate structures: Models for amorphous concentrated liquid and polymer electrolytes (I). *Chem. Mater*. **2003**, *15*, 4679.

(14) Rhodes, C. P.; Frech, R. Local structures in crystalline and amorphous phases of diglyme-$LiCF_3SO_3$ and poly(ethylene oxide)-$LiCF_3SO_3$ systems: Implications for the mechanism of ionic transport. *Macromolecules* **2001**, *34*, 2660.

(15) Andreev, Y. G.; Seneviratne, V.; Khan, M.; Henderson, W. A.; Frech, R. E.; Bruce, P. G. Crystal structures of poly(ethylene oxide)$_3$:$LiBF_4$ and (diglyme)$_n$:$LiBF_4$ (n = 1,2). *Chem. Mater*. **2005**, *17*, 767.

(16) Harvey, S.; Kildea, J. D.; Skelton, B. W.; White, A. H. Lewis-base adducts of main group metal compounds. Adducts of lithium(1) perchlorate with o-methyl-substituted monodentate pyridine bases of increasing bulk. *Aust. J. Chem.* **1992**, *45*, 1135.

(17) Pejov, L.; Petrusevski, V. M. Fourier transform infrared study of perchlorate ($^{35}ClO_4^-$ and $^{37}ClO_4^-$) anions isomorphously isolated in potassium permanganate matrix. Vibrational anharmonicity and pseudo-symmetry effects. *J. Phys. Chem. Solids* **2002**, *63*, 1873.

(18) James, D. W.; Mayes, R. E. Ion-ion-solvent interactions in solution. 8. Spectroscopic studies of the lithium perchlorate/*N*,*N*-dimethylformamide system. *J. Phys. Chem.* **1984**, *88*, 637.

(19) James, D. W.; Mayes, R. E. Ion-ion-solvent interactions in solution. I. Solution of $LiClO_4$ in acetone. *Aust. J. Chem.* **1982**, *35*, 1785.

(20) Chabanel, M.; Touaj, K. Aggregation of perchlorates in aprotic donor solvents. Part 1. Lithium and sodium perchlorates. *J . Chem. Soc., Faraday Trans.* **1996**, *92*, 4199.

(21) Chabanel, M.; Touaj, K. Aggregation of perchlorates in aprotic donor solvents. Part 2. Alkaline-earth metal perchlorates. *J . Chem. Soc., Faraday Trans.* **1996**, *92*, 4207.

(22) Miller, A. G.; Macklin, J. W. Vibrational spectroscopic studies of sodlum perchlorate contact ion pair formatlon in aqueous solution. *J. Phys. Chem.* **1985**, *89*, 1193.

(23) Seo, D. M. *et al*., unpublished data for $(DMP)_2$:$LiBF_4$ solvate at -80°C for 400-600 cm^{-1} region (given in Appendix).

(24) Seo, D. M. *et al*., unpublished data for $(DMP)_2$:$LiBF_4$ solvate at -80°C for 900 cm^{-1} region (given in Appendix).

(25) Seo, D. M. *et al*., unpublished data for $(12C4)_2$:LiTFSI solvate at -80°C for 400-600 cm^{-1} region (given in Appendix).

(26) Xuan, X.; Zhang, H.; Wang, J.; Wang, H. Vibrational spectroscopic and density functional studies on ion solvation and association of lithium tetrafluorobrate in acetonitrile. *J. Phys. Chem. A* **2004**, *108*, 7513.

(27) Hyodo, S. A.; Okabayashi, K. Raman intensity study of local structure in non-aqueous electrolyte solutions. II. Cation--solvent interaction in mixed solvent systems and selective solvation. *Electrochim. Acta* **1989**, *34*, 1557.

(28) Seo, D. M. *et al*., unpublished data for $(PMDETA)_1$:LiTFSI solvate at -80°C for 890-990 cm^{-1}. (given in Appendix).

(29) James, D. W.; Mayes, R. E. Ion-ion-solvent interactions in solution. II. Solutions of $LiClO_4$ in diethyl ether. *Aust. J. Chem.* **1982**, *35*, 1785.

(30) Leong, W. H.; James, D. W. Vibrational spectra of anhydrous lithium perchlorate in crystalline and molten states. *Aust. J. Chem.* **1969**, *22*, 499.

Chapter 4. Thermal and Vibrational Analysis of Linear Carbonates and Carboxylic Esters with $LiClO_4$

4.1 Introduction

Mixtures of linear solvents (linear carbonates and carboxylic esters) and $LiClO_4$ have been analyzed using phase diagrams and Raman spectra. Previously, a number of researchers have studied mixtures of $LiClO_4$ with linear and cyclic carbonates to explore liquid electrolyte properties.[1-6] A combination of phase diagrams, Raman spectroscopy and solvate crystal structures has been used to study binary mixtures of $LiClO_4$ with linear carbonates or carboxylic esters, however, for the first time in this study. The solvents studied are DMC, DEC, MA and EA. DMC and DEC are the most commonly used linear carbonates for current state-of-the-art electrolytes for Li-ion batteries.[7,8] MA and EA are chosen because these carboxylic esters have structures similar to DMC and DEC (Table 4-1). The main difference is they have one oxygen less compared to the carbonates. The four solvents studied will, therefore, aid in understanding how small variations in solvent structure influence the distribution of the various solvate species present in the solvent−LiX mixtures. $LiClO_4$, though not used in commercial Li-ion battery electrolytes, is widely used for laboratory research.[9-11]

Table. 4-1. Names, structures and properties of the solvents examined.[8,12]

Name of the Solvents	Molecular Weight	T_m	T_b
dimethyl carbonate (DMC)	90.08	6	90
diethyl carbonate (DEC)	118.13	-74	126-128
methyl acetate (MA)	74.08	-98	57-58
ethyl acetate (EA)	88.11	-84	77

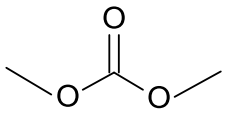

dimethyl carbonate
(DMC)

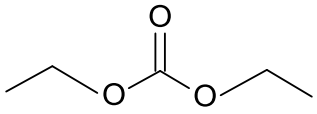

diethyl carbonate
(DEC)

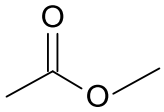

methyl acetate
(MA)

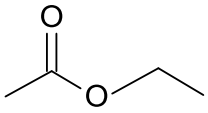

ethyl acetate
(EA)

4.2 Results and Discussion

4.2.1 DMC-$LiClO_4$

DMC has a structure similar to DEC, but with shorter alkyl chains. From Figures 4-1a and 4-1b, pure DMC has a T_m at 6°C and a low energy solid-solid phase transition at -52°C.[12] As the concentration of $LiClO_4$ increases, the solvent peaks get smaller and shift to lower temperatures due to the availability of less bulk solvent for crystallization. No solvate crystalline phases are observed for the $(DMC)_n$-$LiClO_4$ mixtures. The concentrated mixtures remain amorphous. It seems that the solvent and the ions fail to pack in a favorable way to

form an ordered crystalline solvate structure. Figure 4-2a gives the anion vibration band for liquid $(DMC)_n$-$LiClO_4$ mixtures at 20°C. Pure DMC has a CH_3-O stretching band at around 916 cm^{-1}, but Li^+ cation coordinated DMC has a band at 933 cm^{-1} which overlaps with the Cl-O stretching (υ_1) vibrational band for the ClO_4^- SSIP solvates.[13] Thus, deconvolution of the anion vibrational bands to estimate the percentages of different solvates is not possible for the $(DMC)_n$-$LiClO_4$ mixtures. A general trend, however, can be noticed from Figure 4-2a. Even for highly concentrated mixtures ($n \leq 3$), there are Raman bands at approximately 933 cm^{-1}. This implies that the solvent competes effectively with the anions to coordinate Li^+ cations. It is expected that the C=O group of DMC will coordinate the Li^+ cations, but the carbonyl frequency band for DMC is not significantly affected by Li^+ cation coordination (Figure 4-3a).

4.2.2 DEC-$LiClO_4$

The DSC heating traces and the corresponding phase diagram for $(DEC)_n$-$LiClO_4$ mixtures are given in Figures 4-1c and 4-1d, respectively. The concentrated mixtures ($n < 4$) seem to produce metastable phases.[14] The mixtures were therefore cycled repeatedly at low temeprature to form thermodynamically favored, reproducible equilibrium phases suitable for preparing the phase diagram.[14] From the phase diagram, pure DEC has a T_m at -74°C.[8] With the addition of $LiClO_4$, new phases start to form, giving three distinct phases for 3/1, 2/1 and 1/1 compositions (i.e., $(DEC)_3$:$LiClO_4$, $(DEC)_2$:$LiClO_4$ and $(DEC)_1$:$LiClO_4$). It was not

possible to isolate the 3/1 phase since it has a very low T_m (~ -40°C). The structure for the 2/1 phase is reported in Figure 4-2a and the structure of 1/1 phase was reported in Chapter 3.

Raman data for the anion vibrational bands at -100°C is given in Figure 4-5a. All of the mixtures are solid at this temperature. Pure DEC has a CH_3-O stretching vibration band at 901 cm^{-1}, but when it coordinates a Li^+ cation, it shifts to slightly higher values at 910-915 cm^{-1}.[13] For dilute mixtures (n > 3), therefore, two bands are observed: one broad band which is a combination of uncoordinated and coordinated DEC and another at around 933 cm^{-1}. From the analysis of ClO_4^- anion coordination in Chapter 3, this band is attributed to SSIP solvates. The 3/1 solvate, as shown in the phase diagram, is thus a SSIP solvate. For ClO_4^- SSIP solvates, there should also be a very weak band at 911 cm^{-1} because of the $2\upsilon_2$ overtone in Fermi resonance with the υ_1 vibration of ClO_4^- anion.[15] This band, however, is not observed since it overlaps with the coordinated DEC band. From the phase diagram, for 2 < n < 3, 3/1 and 2/1 solvates are present in the mixtures. In case of the n = 2.78 sample, for example, the band at 911 cm^{-1} is due to coordinated DEC, while the two bands at 933 and 940 cm^{-1} correspond to 3/1 and 2/1 solvates, respectively. The latter band for the 2/1 solvate agrees well with the crystal structure of the $(DEC)_2$:$LiClO_4$ solvate. For more concentrated mixtures (n < 2), the intensity of the coordinated solvent peak decreases significantly because there is less solvent present and the SSIP band disappears. Instead, a new band appears at around 955 cm^{-1} in addition to the AGG-I band at 940 cm^{-1}. From the work in Chapter 3, the band at 955 cm^{-1} is assigned to the AGG-II solvate $(DEC)_1$:$LiClO_4$. The Raman spectra for

the solid mixtures, therefore, are in very good agreement with the phase diagram for the crystalline samples.

Raman data for the anion vibrational bands at 20°C is given in Figure 4-5b. For $n \geq 2$, all of the mixtures are liquid at this temperature. In comparison to the Raman data at -100°C, the plots for the liquid mixtures are broad indicating that the liquid samples consist of a mixture of different solvate species. Bands appear at approximately 932, 937 and 944-946 cm^{-1}, corresponding to SSIP, CIP-I and AGG-I, respectively. Even though the Raman bands for crystalline SSIP and AGG-I solvates match well with those of the liquid mixtures, the Raman bands for CIP-I in the liquid mixtures seem to shift slightly to lower wavenumbers as compared to the crystalline solvates. Deconvolution of the Raman bands for the $(DEC)_n$-$LiClO_4$ mixtures provides an estimate of the amount of different solvates present in the liquid mixtures at 20°C (Figure 4-6a). CIP solvates seem to dominate the $(DEC)_n$−$LiClO_4$ liquid mixtures even for very dilute concentrations. The amount of AGG-I solvates increases with increasing concentration, but no AGG-II species are found over the calculated concentration range. Interestingly, very small amount of SSIP solvates are observed in the liquid mixtures even though the solid state shows a Raman peak for SSIP solvates up to $n > 4$. This indicates that when the solid melts, the solvent molecules are replaced by the anions in the Li^+ cation coordination sphere forming CIPs and AGG solvates. Lower temperature allows the solvent to compete more efficiently with the anions to form SSIP solvates, while higher temperature favors increased aggregation.[16] One limitation of this analysis is the assumption made during the deconvolution of the anion bands. The integrated intensity of a Raman band is

proportional to the concentration of the scattering species and in the calculation it is assumed that the proportionality constant is the same for all of the different kinds of solvates, i.e., they all have equivalent Raman activity.[15] Fig. 4-3b gives the Raman band for the carbonyl C=O vibration for the solvent. Pure DEC has a peak at around 1742 cm^{-1}.[17] The crystal solvate structures show that the Li^+ cation is coordinated by the carbonyl oxygen, but the carbonyl vibration band is not significantly affected by the Li^+ cation coordination even at very high concentrations such as n = 2.

4.2.3 MA-$LiClO_4$

The DSC heating traces and the phase diagram for $(MA)_n$-$LiClO_4$ mixtures (Figures 4-1e and 4-1f) indicate that there are four solvate phases with 5/1, 3/1, 2/1 and 1/1 composition. The 5/1 solvate phase has a very low T_m and so it was not possible to form the single crystals for this phase for structural analysis. The solvate may have a crystal structure similar to that of $(AN)_5$:$LiPF_6$ (Figure 4-4b) in which four AN solvent molecules are coordinated to one Li^+ cation and the remaining solvent molecule remains uncoordinated. An eutectic composition is also present at about x = 0.40 (Figure 4-1f).

Figure 4-5b gives the Raman plots for the $(MA)_n$-$LiClO_4$ mixtures at -100°C when all of the mixtures are solid. As expected from the phase diagram, there is only one peak for dilute mixtures (n > 5) at approximately 933 cm^{-1} corresponding to a SSIP solvate. From the Raman data, the solvate with a 3/1 composition is likely to be a CIP-I solvate because of the presence of a peak at 939 cm^{-1}. For 3 < n < 5, two peaks are observed corresponding to the

Figure 4-1. DSC heating traces of (a) $(DMC)_n$-$LiClO_4$, (c) $(DEC)_n$-$LiClO_4$, (e) $(MA)_n$-$LiClO_4$, (g) $(EA)_n$-$LiClO_4$ and phase diagrams of (b) $(DMC)_n$-$LiClO_4$, (d) $(DEC)_n$-$LiClO_4$, (f) $(MA)_n$-$LiClO_4$ and (h) $(EA)_n$-$LiClO_4$ mixtures. (the crossmarks indicate fully amorphous phases, while the triangles indicate partially crystalline phases).

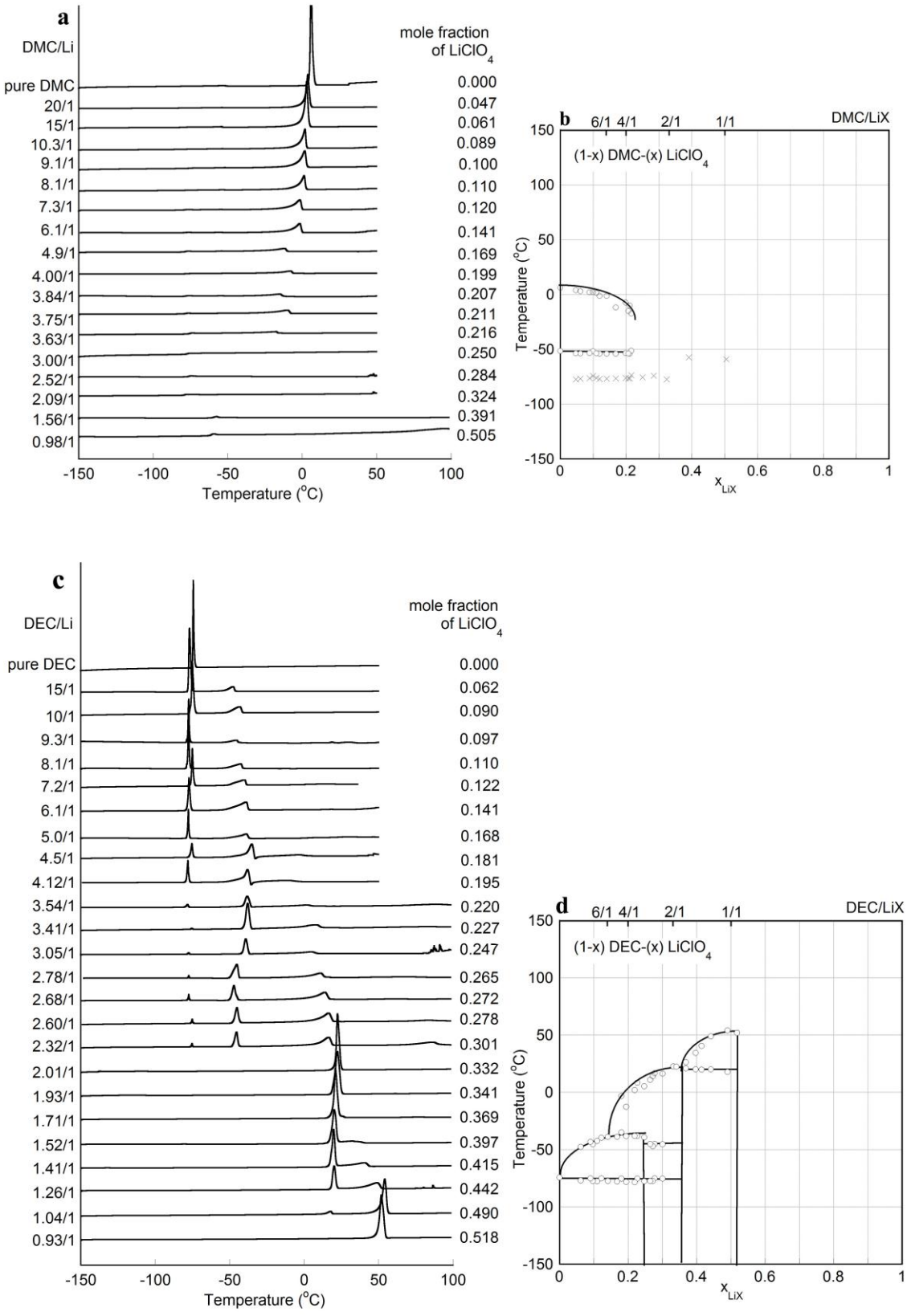
a
DMC/Li
mole fraction of LiClO4
pure DMC 0.000
20/1 0.047
15/1 0.061
10.3/1 0.089
9.1/1 0.100
8.1/1 0.110
7.3/1 0.120
6.1/1 0.141
4.9/1 0.169
4.00/1 0.199
3.84/1 0.207
3.75/1 0.211
3.63/1 0.216
3.00/1 0.250
2.52/1 0.284
2.09/1 0.324
1.56/1 0.391
0.98/1 0.505
-150 -100 -50 0 50 100
Temperature (°C)
b
6/1 4/1 2/1 1/1
DMC/LiX
(1-x) DMC-(x) LiClO4
Temperature (°C)
150 100 50 0 -50 -100 -150
0 0.2 0.4 0.6 0.8 1
xLiX
c
DEC/Li
mole fraction of LiClO4
pure DEC 0.000
15/1 0.062
10/1 0.090
9.3/1 0.097
8.1/1 0.110
7.2/1 0.122
6.1/1 0.141
5.0/1 0.168
4.5/1 0.181
4.12/1 0.195
3.54/1 0.220
3.41/1 0.227
3.05/1 0.247
2.78/1 0.265
2.68/1 0.272
2.60/1 0.278
2.32/1 0.301
2.01/1 0.332
1.93/1 0.341
1.71/1 0.369
1.52/1 0.397
1.41/1 0.415
1.26/1 0.442
1.04/1 0.490
0.93/1 0.518
-150 -100 -50 0 50 100
Temperature (°C)
d
6/1 4/1 2/1 1/1
DEC/LiX
(1-x) DEC-(x) LiClO4
Temperature (°C)
150 100 50 0 -50 -100 -150
0 0.2 0.4 0.6 0.8 1
xLiX

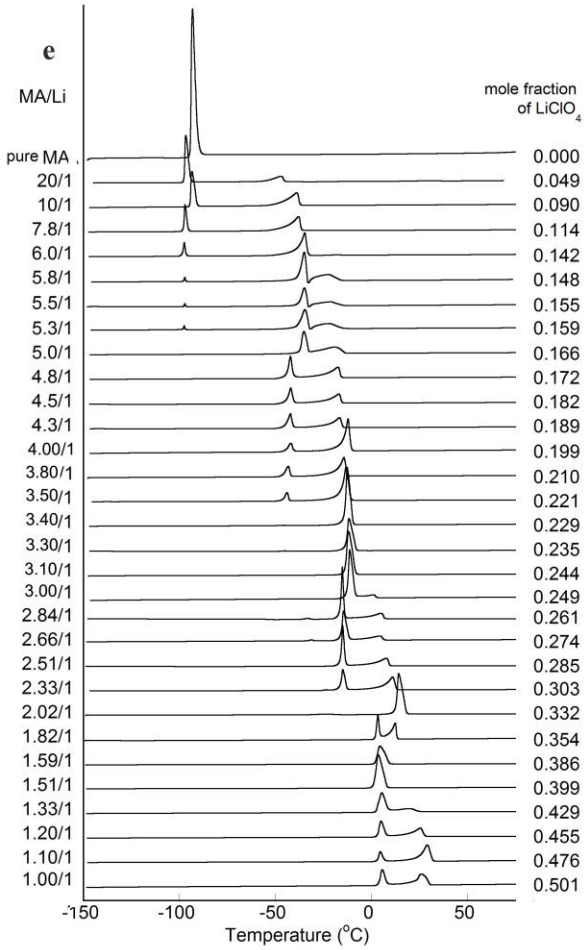
e
MA/Li
mole fraction of LiClO4
pure MA 0.000
20/1 0.049
10/1 0.090
7.8/1 0.114
6.0/1 0.142
5.8/1 0.148
5.5/1 0.155
5.3/1 0.159
5.0/1 0.166
4.8/1 0.172
4.5/1 0.182
4.3/1 0.189
4.00/1 0.199
3.80/1 0.210
3.50/1 0.221
3.40/1 0.229
3.30/1 0.235
3.10/1 0.244
3.00/1 0.249
2.84/1 0.261
2.66/1 0.274
2.51/1 0.285
2.33/1 0.303
2.02/1 0.332
1.82/1 0.354
1.59/1 0.386
1.51/1 0.399
1.33/1 0.429
1.20/1 0.455
1.10/1 0.476
1.00/1 0.501
-150 -100 -50 0 50
Temperature (°C)

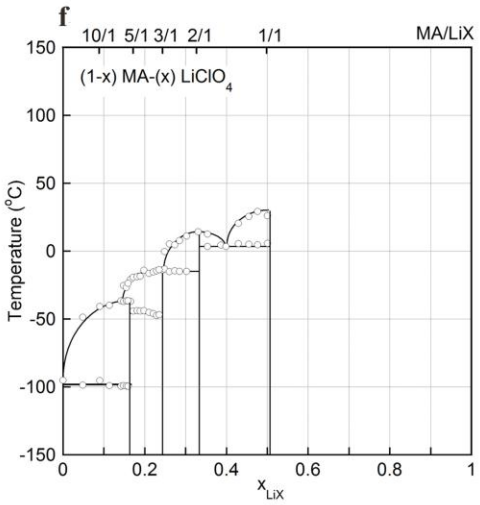
f
10/1 5/1 3/1 2/1 1/1 MA/LiX
(1-x) MA-(x) LiClO4
Temperature (°C)
150 100 50 0 -50 -100 -150
0 0.2 0.4 0.6 0.8 1
xLiX

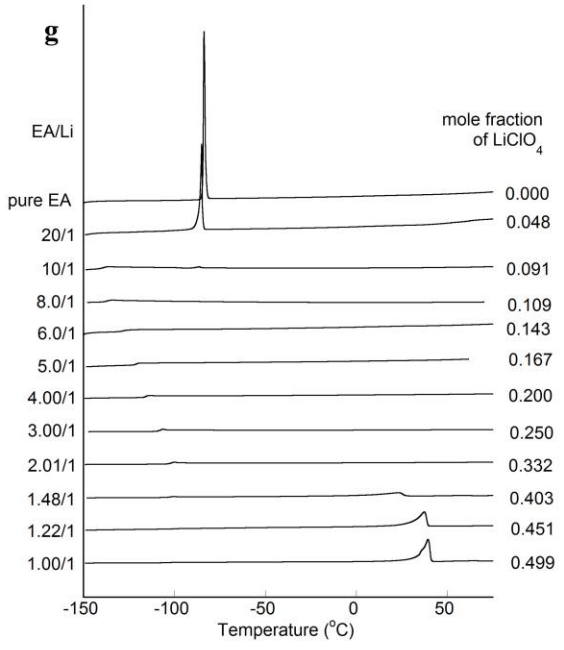
g
EA/Li
mole fraction of LiClO4
pure EA 0.000
20/1 0.048
10/1 0.091
8.0/1 0.109
6.0/1 0.143
5.0/1 0.167
4.00/1 0.200
3.00/1 0.250
2.01/1 0.332
1.48/1 0.403
1.22/1 0.451
1.00/1 0.499
-150 -100 -50 0 50
Temperature (°C)

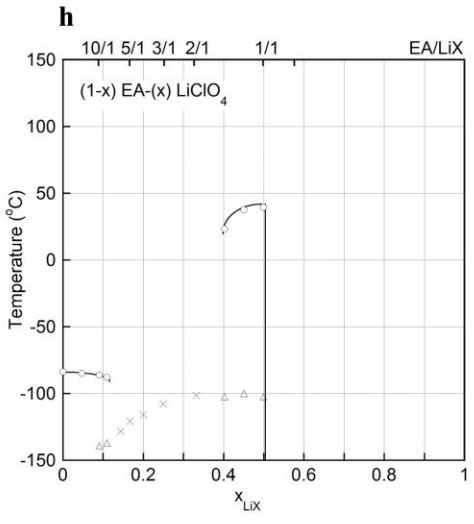
h
10/1 5/1 3/1 2/1 1/1 EA/LiX
(1-x) EA-(x) LiClO4
Temperature (°C)
150 100 50 0 -50 -100 -150
0 0.2 0.4 0.6 0.8 1
xLiX

5/1 and 3/1 phases as expected from the phase diagram (the n = 3.25 mixture gives a shoulder corresponding to SSIP solvates). For n = 2.5, the peak for the SSIP solvate disappears, but a new peak, characteristic of AGG-I solvates, arises at about 944 cm^{-1}. A sharp peak at around 944 cm^{-1} for n = 2, indicates that the 2/1 solvate is an AGG-I solvate. For more concentrated mixtures, a peak at 953 cm^{-1}, corresponding to a $(MA)_1$:$LiClO_4$ AGG-II solvate, is observed. The Raman data is thus in very good agreement with the phase diagram. Figure 4-4c gives the Raman plots for the $(MA)_n$-$LiClO_4$ mixtures at 20°C. At this temperature, all of the mixtures with $n \geq 2$ are liquid. There are Raman bands at 933, 937, 945 and 954 cm^{-1} corresponding to SSIP, CIP-I, AGG-I and AGG-II solvates, respectively. From a visual inspection of the bands, it is evident that the mixtures contain SSIP solvates even at very high concentration and increasing aggregation occurs as the concentration increases. Band deconvolution of the Raman bands for the liquid mixtures yields the amount of different solvates in the mixtures (Figure 4-6b). Again, this determination assumes that all of the different solvates have equivalent Raman activity. From Figure 4-6b, the amount of SSIP solvates decreases with increasing salt concentration, but SSIP solvates are still present even for very concentrated mixtures up to n = 3. CIP solvates seem to be the dominant solvate species and AGG-I solvates appear for mixtures with $n \geq 6$. AGG-II solvates are observed only for n = 2. A comparison of Figures 4-6a and 4-6b shows some interesting features for the different solvent mixtures. CIP solvates seem to be the most common solvate species for the liquids at 20°C for both DEC and MA. $(DEC)_n$-$LiClO_4$ mixtures have SSIPs only for very dilute mixtures, i.e., n = 20, but $(MA)_n$-$LiClO_4$ mixtures have SSIP solvates even for very

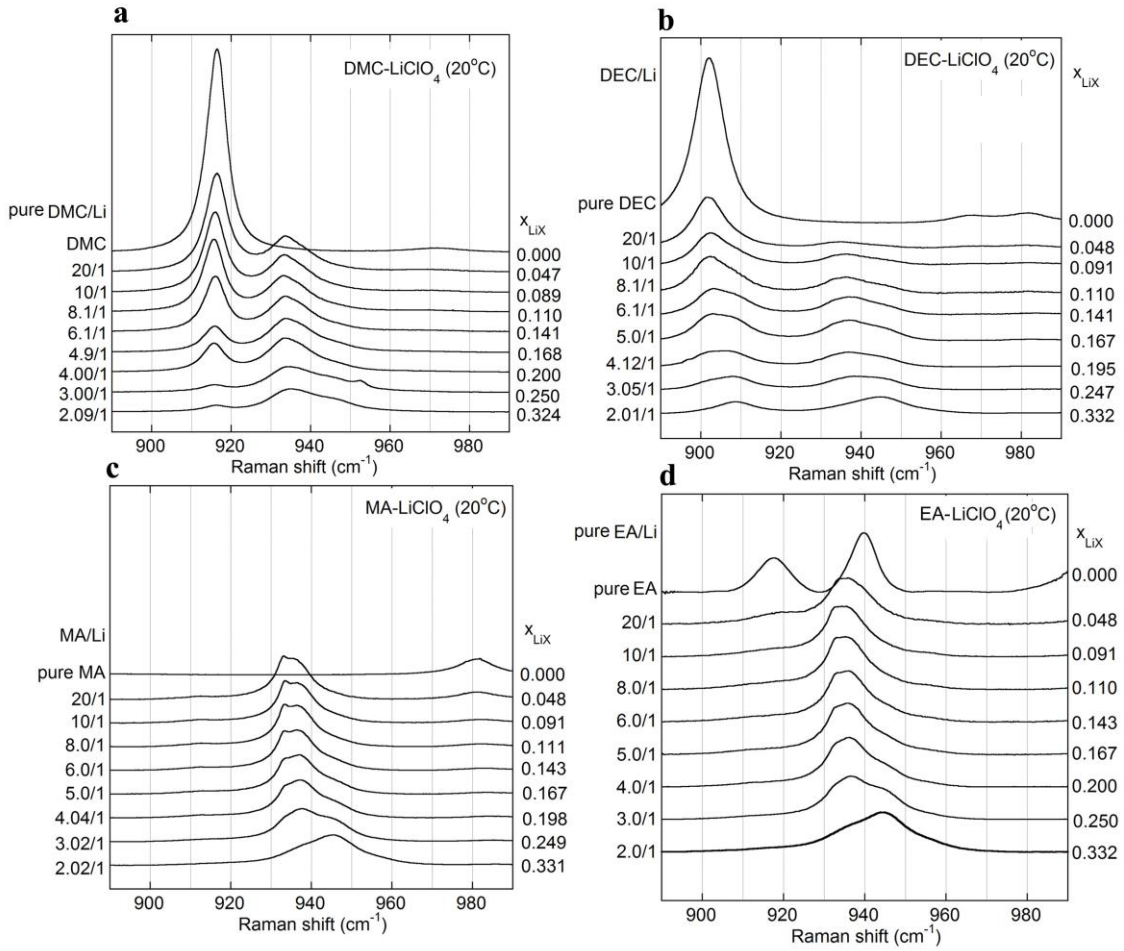

Figure 4-2. Anion vibration bands for (a) $(DMC)_n$-$LiClO_4$, (b) $(DEC)_n$-$LiClO_4$, (c) $(MA)_n$-$LiClO_4$ and (d) $(EA)_n$-$LiClO_4$ mixtures at 20°C.

concentrated mixtures. This shows that, in the liquid mixtures, MA competes more effectively with the anion for Li^+ cation coordination than DEC. As for DEC and DMC, the Raman band for the carbonyl group of MA is not significantly affected by Li^+ coordination. At very high concentrations (i.e., n = 3.02 and 2.02), the bands become broader.

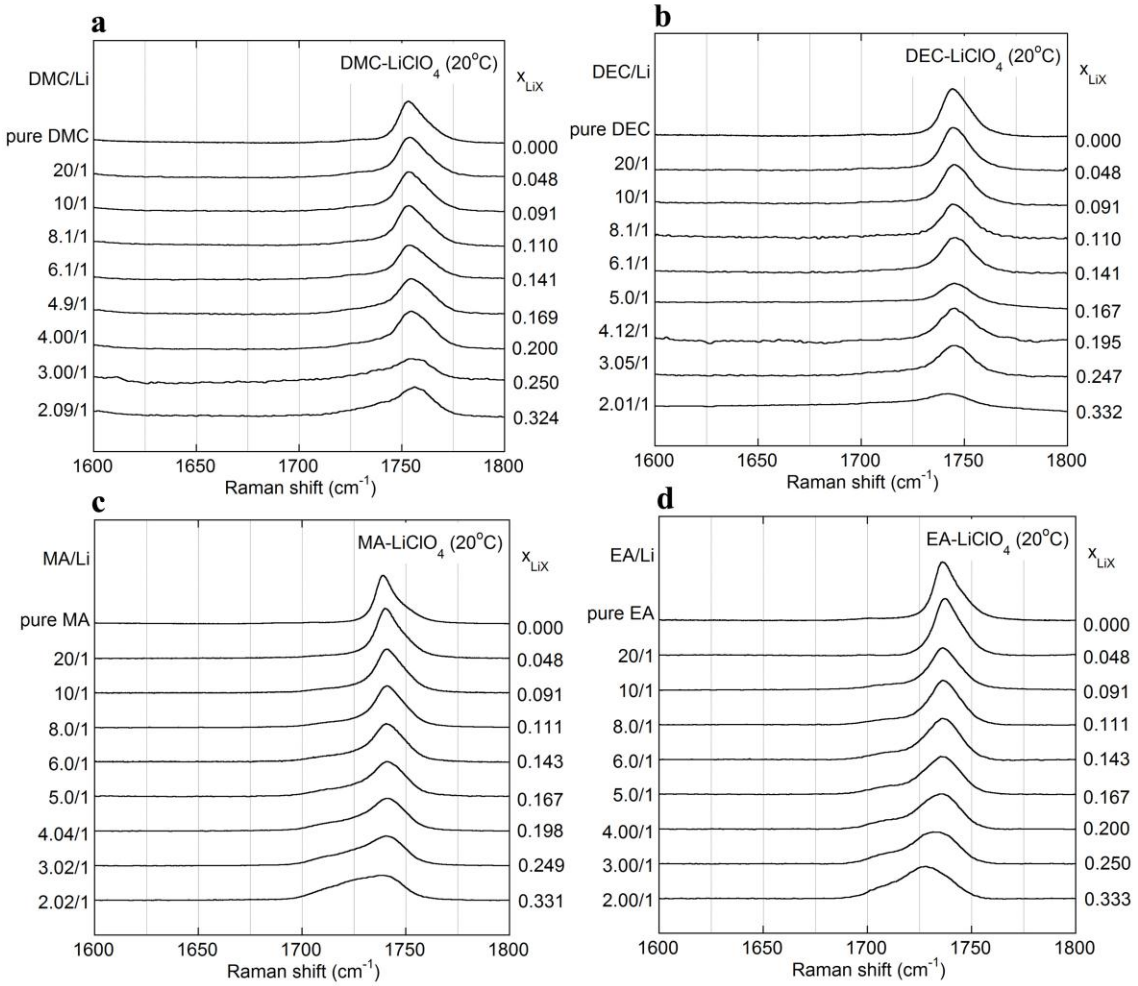

Figure 4-3. Raman bands for C=O vibration in (a) $(DMC)_n$-$LiClO_4$, (b) $(DEC)_n$-$LiClO_4$, (c) $(MA)_n$-$LiClO_4$ and (d) $(EA)_n$-$LiClO_4$ mixtures at 20°C.

4.2.4 EA-$LiClO_4$

The DSC heating traces and the corresponding phase diagram for the $(EA)_n$-$LiClO_4$ mixtures are given in Figures 4-1g and 4-1h. For very dilute mixtures, some of the solvent may be crystallized, but for $2 \leq n < 10$, it is not possible to crystallize the mixtures even after

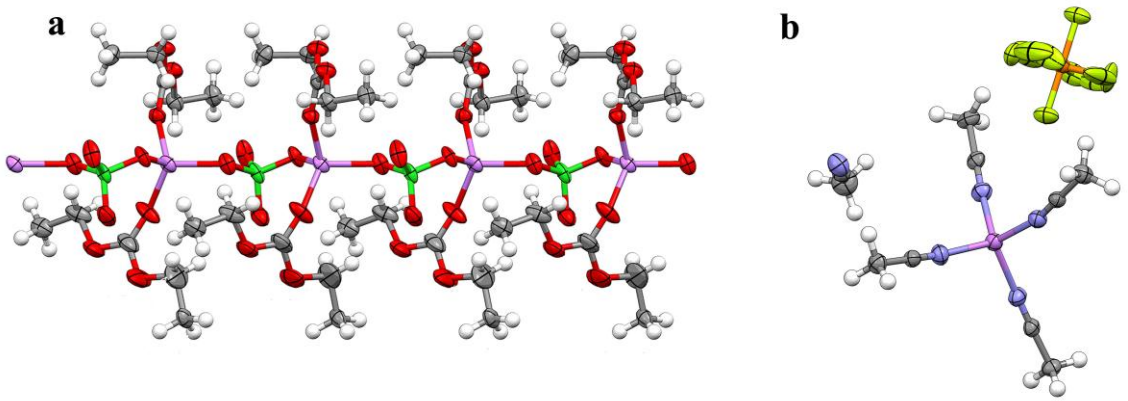

Figure 4-4. Li^+ cation coordination in crystalline solvate structures (a) $(DEC)_2$:$LiClO_4$ and (b) $(AN)_5$:$LiPF_6$. (Li-purple, O-red, N-blue, Cl-dark green, P-orange, F-light green)

extensive heating/cooling cycles, resulting in a 'crystallinity gap'. The probable reason for such a crystallinity gap may be that the solvates found in the amorphous phase do not pack together in an energetically favorable manner in a crystalline phase, thereby inhibiting the nucleation and growth of such phases.[16] The glass transition temperature, T_g (indicated by cross marks for the fully amorphous phases and by triangles for the partially crystalline phases) increases up to n = 2.01, but after that it becomes constant. The amorphous phase becomes more aggregated with increasing $LiClO_4$ concentration, resulting in a subsequent increase in the T_g. At n > 2, a portion of the mixtures starts to crystallize and an amorphous phase of constant composition (hence constant T_g) remains. The phase that crystallizes out has a 1/1 composition. Single crystals of $(EA)_1$:$LiClO_4$ which are stable at room temperature were formed by storing an $(EA)_n$-$LiClO_4$ (n = 2) mixture in the refrigerator at 4°C. The structure of $(EA)_1$:$LiClO_4$ is reported in Chapter 3.

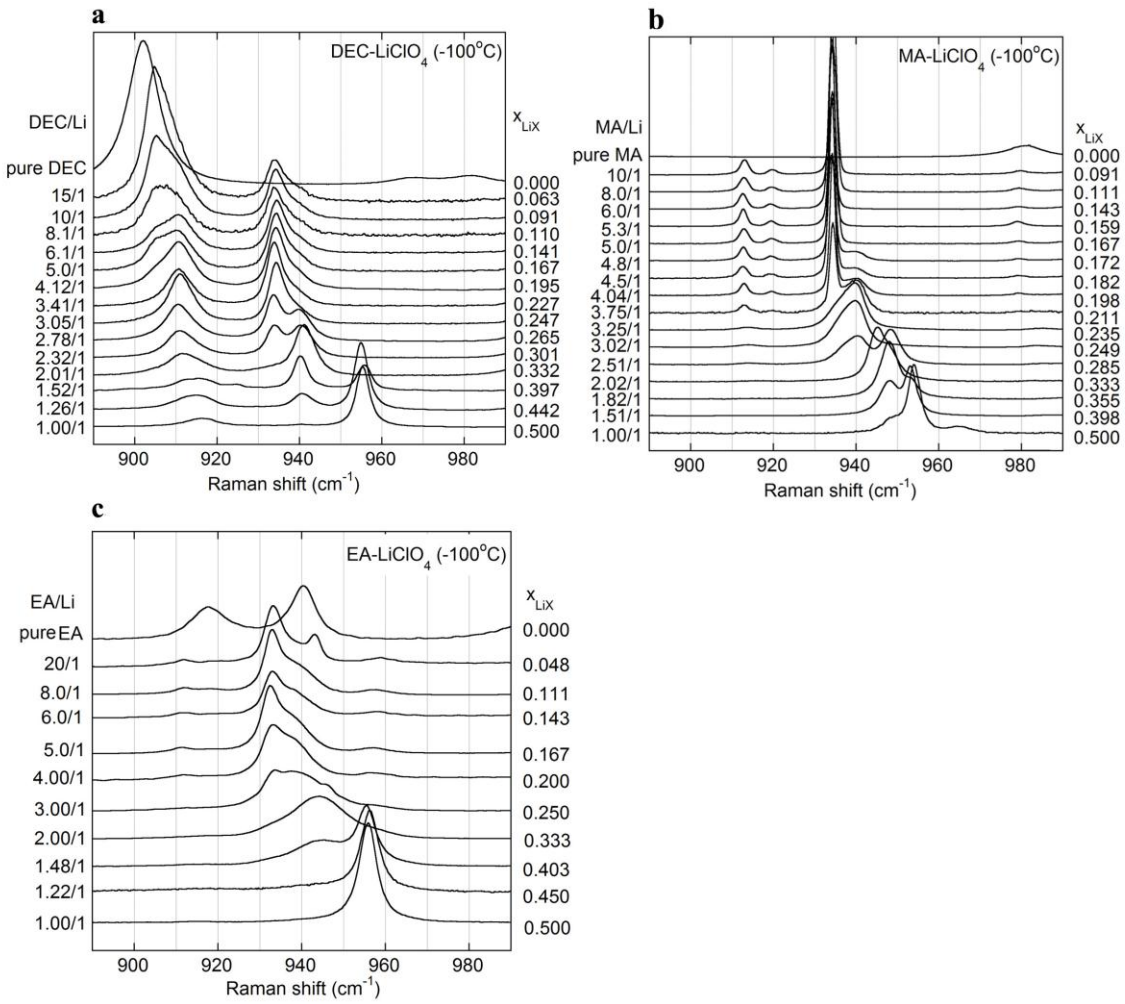

Figure 4-5. Variation of anion vibration bands with concentration for (a) $(DEC)_n$-$LiClO_4$ (b) $(MA)_n$-$LiClO_4$ and (c) $(EA)_n$-$LiClO_4$ mixtures at -100°C.

The anion Raman bands for $(EA)_n$-$LiClO_4$ mixtures at -100°C are given in Figure 4-5c. Pure EA has bands at around 918 and 939 cm^{-1}. The solvent band at 939 cm^{-1} overlaps with the anion band for CIP-I solvates. For n = 20, where a portion of the solvent is crystallized, the Raman bands for coordinated EA shift to higher wavenumbers giving bands which overlap with the SSIP and AGG-I solvates, respectively. The Raman bands become broader

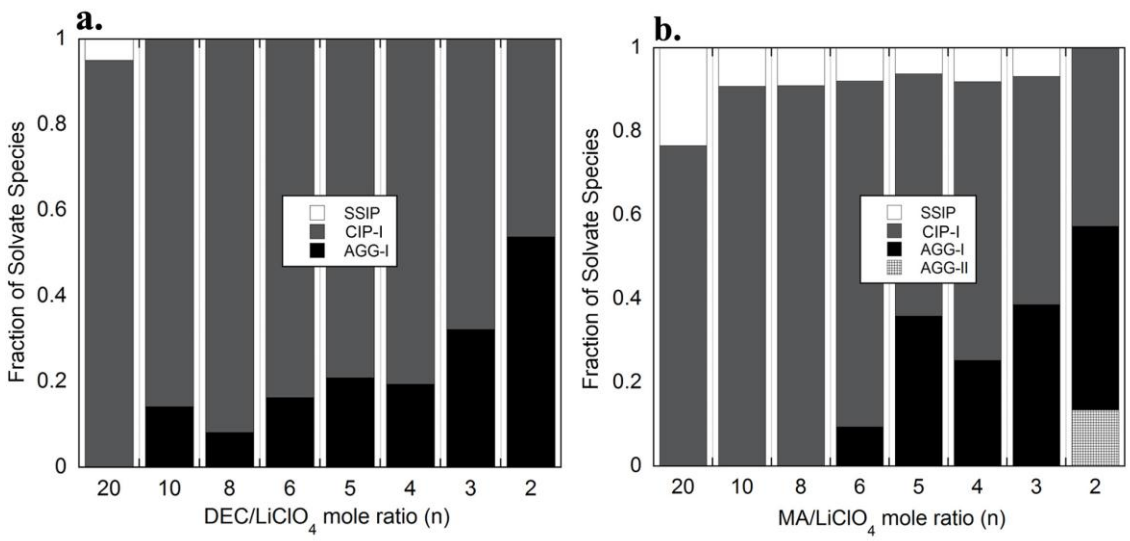

Figure 4-6. Fraction of solvates in (a) $(DEC)_n$-$LiClO_4$ and (b) $(MA)_n$-$LiClO_4$ mixtures.

and gradually shifts to higher wavenumbers for the amorphous region (i.e., $2 \leq n < 20$). For n = 1.48, where part of the sample crystallizes, a sharp peak at 955 cm^{-1} agrees with the presence of the $(EA)_1$:$LiClO_4$ AGG-II solvates in the mixture at a temperature of -100°C. The Raman spectra for $(EA)_n$-$LiClO_4$ mixtures at 20°C is given in Fig. 4-2d. The overlap of the anion bands with the coordinated and uncoordinated solvent bands make it impossible to use band deconvolution to approximate the fraction of different solvate species present in the liquid mixtures. Pure EA has a carbonyl group vibration band at 1742 cm^{-1}.[17] The carbonyl vibrational band of EA was not significantly affected by the Li^+ coordination except for very concentrated mixtures where the band was slightly distorted, giving rise to a very broad shoulder at around 1700 cm^{-1}.

4.3 Conclusions

Phase diagrams for $(DMC)_n$-$LiClO_4$, $(DEC)_n$-$LiClO_4$, $(MA)_n$-$LiClO_4$ and $(EA)_n$-$LiClO_4$ mixtures were prepared. Even though DMC and DEC have very similar structures, their phase behavior is quite different. $(DMC)_n$-$LiClO_4$ mixtures gave only amorphous phases, while $(DEC)_n$-$LiClO_4$ mixtures formed three crystalline phases with 3/1, 2/1 and 1/1 compositions. The crystalline solvate structures of $(DEC)_2$:$LiClO_4$ (AGG-I) and $(DEC)_1$:$LiClO_4$ (AGG-II) solvates were determined. $(MA)_n$-$LiClO_4$ and $(EA)_n$-$LiClO_4$ mixtures also showed very different phase behavior even though MA and EA have similar structures. Unlike $(MA)_n$-$LiClO_4$ mixtures, which gave crystalline phases with 5/1, 3/1, 2/1 and 1/1 compositions, $(EA)_n$-$LiClO_4$ mixtures exhibited a 'crystallinity gap' with one crystalline solvate with a 1/1 composition. The AGG-II structure of $(EA)_1$:$LiClO_4$ solvate was also determined. Raman spectroscopy was used to study the interaction of the anions and solvents with the Li^+ cations. Raman characterization of ClO_4^- crystalline solvates (Chapter 3) was used to deconvolute the anion Raman bands for the liquid mixtures, where possible. This, in turn, provided an estimation of the fraction of different solvate species present in the solution. It was found that, at 20°C, CIP solvates are the dominant species in both $(DEC)_n$-$LiClO_4$ and $(MA)_n$-$LiClO_4$ mixtures. $(DEC)_n$-$LiClO_4$ mixtures have SSIP solvates only for n = 20, but $(MA)_n$-$LiClO_4$ mixtures have SSIP solvates even for very concentrated mixtures. It was not possible to estimate the amount of solvates in $(DMC)_n$-$LiClO_4$ and $(EA)_n$-$LiClO_4$ mixtures because of the overlap of the coordinated and uncoordinated solvent bands with the anion bands.

References

(1) Qiao, H.-W.; Luan, H.-L.; Zhou, Z.-M.; Yao, W. Vibrational spectroscopic study on ion solvation and association of lithium perchlorate in 4-methoxymethyl-ethylene carbonate. *Chin. J. Chem.* **2007**, *25*, 461.

(2) Brooksby, P. A.; Fawcett, W. R. Infrared (attenuated total reflection) study of propylene carbonate solutions containing lithium and sodium perchlorate. *Spectrochim. Acta, Part A* **2006**, *64*, 372.

(3) Stygar, J.; Zukowska, G.; Wieczorek, W. Study of association in alkali metal perchlorate-poly(ethylene glycol) monomethyl ether solutions by FT-IR spectroscopy and conductivity measurements. *Solid State Ionics* **2005**, *176*, 2645.

(4) Wang, J.; Wu, Y.; Xuan, X.; Wang, H. Ion-molecule interactions in solutions of lithium perchlorate in propylene carbonate + diethyl carbonate mixtures: An IR and molecular orbital study. *Spectrochim. Acta, Part A* **2002**, *58*, 2097.

(5) Wang, Z.; Huang, B.; Xue, R. J.; Chen, L.; Huang, X. Ion association and solvation studies of $LiClO_4$/ethylene carbonate electrolyte by Raman and Infrared spectroscopy. *J. Electrochem. Soc.* **1998**, *145*, 3346.

(6) Klassen, B.; Aroca, R.; Nazri, M.; Nazri, G. A. Raman spectra and transport properties of lithium perchlorate in ethylene carbonate based binary solvent systems for lithium batteries. *J. Phys. Chem. B* **1998**, *102*, 4795.

(7) Morita, M.; Asai, Y.; Yoshimoto, N.; Ishikawa, M. A. Raman spectroscopic study of organic electrolyte solutions based on binary solvent systems of ethylene carbonate with low viscosity solvents which dissolve different lithium salts. *J. Chem. Soc., Faraday Trans.* **1998**, *94*, 3451.

(8) Ding, M. S.; Xu, K.; Zhang, S.; Jow, T. R. Liquid/solid phase diagrams of binary carbonates for lithium batteries. *J. Electrochem. Soc.* **2001**, *148*, A299.

(9) Sawai, K.; Iwakoshi, Y.; Ohzuku, T. Carbon materials for lithium-ion (shuttlecock) cells. *Solid State Ionics* **1994**, *69*, 273.

(10) Uchida, I.; Sato, H., Preparation of binder-Free, thin film $LiCoO_2$ and its electrochemical responses in a propylene carbonate solution. *J. Electrochem. Soc.* **1995**, *142*, L139.

(11) Tarascon, J. M.; Guyomard, D.; Baker, G. L. An update of the Li metal-free rechargeable battery based on $Li_{1+x}Mn_2O_4$ cathodes and carbon anodes. *J. Power Sources* **1993**, *44*, 689.

(12) Xu, K. Nonaqueous liquid electrolytes for lithium-based rechargeable batteries. *Chem. Rev*. **2004**, *104*, 4303.

(13) Doucey, L.; Revault, M.; Lautié, A.; Chaussé, A.; Messina, R. A study of the Li/Li^+ couple in DMC and PC solvents. Part 1. Characterization of $LiAsF_6$/DMC and $LiAsF_6$/PC solutions. *Electrochim. Acta* **1999**, *44*, 2371.

(14) Callister, W. D. *Materials Science and Engineering: An Introduction*. 4th ed.; John Wiley & Sons, Inc: New York, **1997**.

(15) Miller, A. G.; Macklin, J. W. Vibrational spectroscopic studies of sodium perchlorate contact ion pair formation in aqueous solution. *J. Phys. Chem.* **1985**, *89*, 1193.

(16) Henderson, W. A. Glyme—lithium salt phase behavior. *J. Phys. Chem. B* **2006**, *110*, 13177.

(17) Thompson, H. W.; Jameson, D. A. Vibrational frequency and band intensity of the carbonyl group. *Spectrochim. Acta* **1958**, *13*, 236.

Chapter 5. Conclusions

The main objective of this project was to understand the molecular-level interactions occurring in various solvent-LiX mixtures because the interactions between the Li^+ cations, anions and solvent molecules within electrolytes influence bulk electrolyte properties such as viscosity and ionic conductivity.

Initially, Raman spectroscopy was used to characterize $LiClO_4$ solvates with known crystal structures so as to unambiguously assign the Raman bands to specific forms of ClO_4^- coordination to Li^+ cations (Chapter 3). Lassègues *et al.* did a similar preliminary study where the known crystalline solvate structures of glymes with $LiClO_4$ and the structure of pure $LiClO_4$ salt were utilized to establish vibrational assignments for the ClO_4^- anion with SSIP, CIP-I, CIP-II, AGG-I and AGG-III coordination. In the present study, however, numerous ClO_4^- solvates in addition to the glyme-$LiClO_4$ solvates were used to confirm the Raman bands assignments for specific forms of ClO_4^- coordination to Li^+ cations. The crystal structures of some of the solvates characterized were already known and five new solvate structures were determined for this study. In addition, the effect of temperature on the anion vibration bands were also studied. It was found that, on average, for the ClO_4^- anion at a temperature of -100°C, there are bands at 933, 942, 925, 944, 956 and 964 cm^{-1} corresponding to SSIP, CIP-I, CIP-II, AGG-I, AGG-II and AGG-III solvates, respectively. For the SSIP, CIP-I, AGG-I and AGG-III solvates, the peak shifts to slightly lower values as the temperature increases. The peak position for CIP-II and AGG-II solvates, however, moves to higher values with increasing temperature. Further, the Raman bands for CIP-I and

AGG-I are positioned close together, leading to some difficulties in differentiating between these two solvates by Raman spectroscopy. For all the solvates, the peaks become broader as the temperature increases indicating increased disorder of the ClO_4^- anions with increasing temperature.

The information from Chapter 3 was used in Chapter 4 where mixtures of linear solvents—linear carbonates (DMC, DEC) and carboxylic esters (MA, EA)—and $LiClO_4$ were analyzed using phase diagrams and Raman spectroscopy. Phase diagrams for $(DMC)_n$-$LiClO_4$, $(DEC)_n$-$LiClO_4$, $(MA)_n$-$LiClO_4$ and $(EA)_n$-$LiClO_4$ mixtures provided information regarding the kind of solvates present in the mixtures in the solid-state, as well as the solid-liquid phase behavior of the different solvents used when mixed with $LiClO_4$. Raman spectroscopy was used to study the interactions of the anions and solvents with Li^+ cations. Raman characterization of ClO_4^- crystalline solvates (Chapter 3) was used to deconvolute the anion Raman bands for the liquid mixtures, where possible (Chapter 4). This, in turn, provided an estimation of the fraction of different solvate species present in the solution. It was shown that small variations in the solvent structure affect the amount of different solvate species present in the solution. Thus, as demonstrated here, a combination of phase diagrams, Raman spectroscopic analysis and solvate crystal structures provides significant insight regarding the identity of the solvate species present in solution. This, in turn, should help to correlate the molecular-level interactions in solvent-LiX mixtures with the bulk electrolyte properties such as viscosity and conductivity.

Appendix

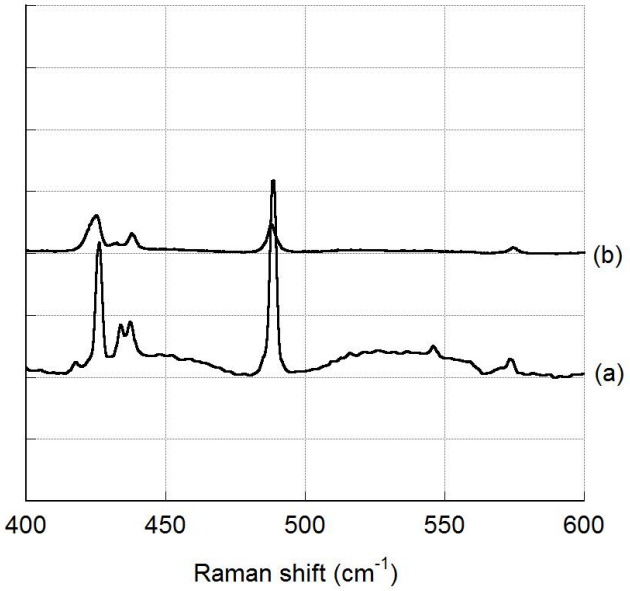

Figure 1. Raman bands for (a) $(DMP)_2$:$LiBF_4$ at -80°C and (b) pure DMP.

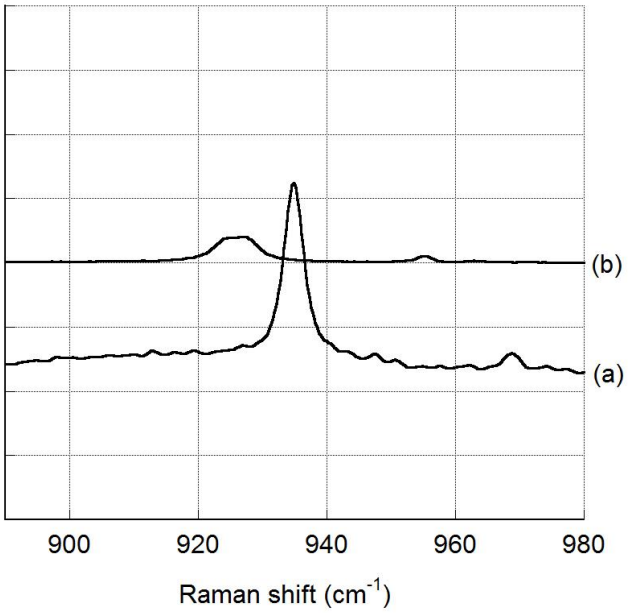

Figure 2. Raman bands for (a) $(DMP)_2$:$LiBF_4$ at -80°C and (b) pure DMP.

Figure 1 shows that pure DMP and coordinated DMP have bands in the 400-600 region which explains the presence of extra bands for $(DMP)_2$:$LiClO_4$:MeOH solvate for υ_2 and υ_4 vibrational modes ($LiBF_4$ has no band in this region). Also coordinated DMP has a peak at around 933 cm^{-1} which explains the presence of a little shoulder for $(DMP)_2$:$LiClO_4$:MeOH solvate at -100°C.

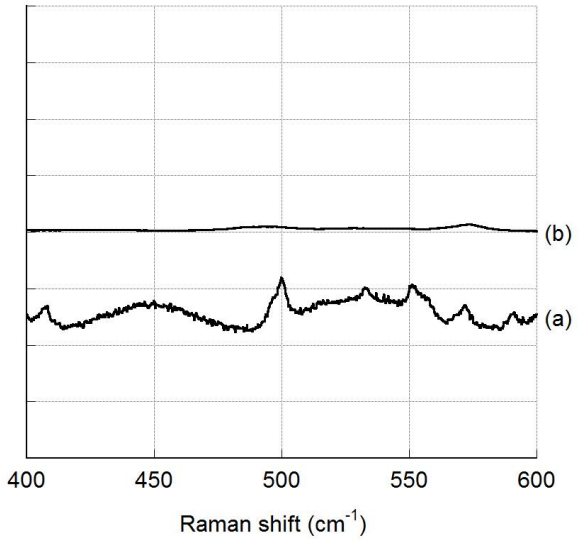

Figure 3. Raman bands for (a) $(12C4)_2$:LiTFSI at -80°C and (b) pure 12C4.

Pure 12C4 has no band in the 400-600 region, but the coordinated 12C4 solvent does have bands in the 400-600 cm^{-1} region (LiTFSI has no bands in this region) (Figure 3). This explains the presence of extra bands for the $(12C4)_{3/2}$:$LiClO_4$ solvate for υ_2 and υ_4 vibrational modes. The peaks for coordinated PMDETA in the 890-990 region (Figure 4) give rise to the asymmetric band for $(PMDETA)_1$:$LiClO_4$ solvate in υ_1 vibrational region.

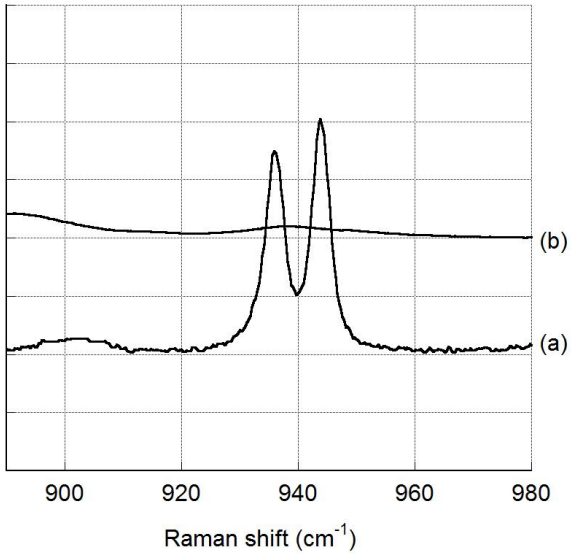

Figure 4. Raman bands for (a) $(PMDETA)_1$:LiTFSI at -80°C and (b) pure PMDETA.